Table 1
Haplotype analysis

	P1	P2	P3	P4	P5	Control[A]
Intron 1, rs2062213	C/C	C/C	C/C	C/C	C/C	C/C (53%)
Intron 1, rs8070945	C/C	C/C	C/C	C/C	C/C	C/C (78%)
Intron 1, rs963988	G/G	G/G	G/G	G/G	G/G	G/G (33%)
Intron 1, rs963987	G/G	G/G	G/G	G/G	G/G	G/G (31%)
Intron 1, rs963986	G/G	G/G	G/G	G/G	G/G	G/G (34%)
Exon 2, 9-bp insertion[B]	no/no	no/no	no/no	no/no	no/no	no/no (72%)
Exon 2, rs9252[B]	C/C	C/C	C/C	C/C	C/C	C/C (78%)
STS-W93348 (bp)	251/253	251/253	251/253	251/253	251/253	251/253/264
D17S1185 (bp)	219/219	170/219	170/219	170/170	170/203	170/203/215/219/225/237

[A]Percentages denote the frequency of the haplotype in the HapMap JPT population. [B]Exon 2 is 3′ noncoding.

muscle mounding was characteristic. Cardiac arrhythmia, transient immunodeficiency, recurrent pneumonia, constipation, and chalasia were variably seen. Available laboratory data in the patients are summarized in Table 3. Metabolic complication was mild, and none of our patients showed marked elevation of fasting glucose levels. The result of oral glucose tolerance tests revealed moderate fasting hyperinsulinemia in P1 and P2 associated with glucose intolerance in P2, but normal levels in P4 (Table 4). High triglyceremia was seen in P4 and P5. Serum creatine kinase (CK) levels were moderately elevated in all patients. Abdominal CT images of P4 revealed marked loss of subcutaneous and intra-abdominal fat (Figure 2, B and C). In addition, his body fat ratio, as determined by whole body dual energy X-ray absorptiometry, was 7.1% (Supplemental Table 1; supplemental material available online with this article; doi:10.1172/JCI38660DS1), while head fat was relatively preserved.

Clinical features of the heterozygous parents. There was no family history of muscular dystrophy or lipodystrophy in P1–P5. Genetic analysis revealed a heterozygous c.696_698insC mutation in both parents of P4. Clinically, both father and mother had hypertension requiring medication, whereas P4 was normotensive. Mild lipid metabolism abnormality and borderline glucose intolerance was also seen (Supplemental Table 2). DNA samples from the other parents were not available.

Loss of PTRF with deficiency or mislocalization of caveolins in skeletal muscle. Biopsied skeletal muscles from P1–P5 showed consistent findings, with chronic dystrophic changes including marked variation in muscle fiber size, increased number of fibers containing internalized nuclei, a few necrotic and regenerating fibers, and increased interstitial fibrosis (Figure 2D and Supplemental Figure 1). Intramuscular lipid droplets, as visualized by oil red O staining, were not increased (Figure 2D).

Immunohistochemistry demonstrated that the PTRF antibodies A301-269A and A301-271A (which recognize the N- and C-terminal regions of the protein, respectively; Figure 1B) showed sarcolemmal membrane staining of muscle fibers, with stronger immunoreaction at intramuscular blood vessels in control muscles (Figure 3A). Caveolin-3 was clearly observed at sarcolemma, whereas caveolin-1 and -2 were present only in blood vessels. In contrast, muscles from P1–P5 showed barely detectable immunoreaction to both PTRF antibodies (Figure 3A). Caveolin-3 immunoreactivity was greatly reduced in the sarcolemma, but cytoplasmic staining was remarkably increased. This caveolin-3 staining pattern was similar to that seen in the patients with muscular dystrophy

Table 2
Clinical summary

	P1	P2	P3	P4	P5
Age/sex	8-yr-old female	14-yr-old female	10-yr-old male	27-yr-old male	24-yr-old male
Height, body weight	124 cm, 21.3 kg	149 cm, 40.5 kg	NA	164 cm, 49.0 kg	152 cm, 40 kg
Lipodystrophy	Generalized	Generalized	Generalized	Generalized	Generalized
Mental retardation	No	No	No	No	No
Acanthosis nigricans	No	No	No	No	No
Liver/spleen	Hepatosplenomegaly	Fatty liver	NA	Hepatosplenomegaly	No
Endocrine abnormalities	Reduced growth hormone secretion	NA	NA	Accelerated bone age, acromegaloid features, no androgynism	Acromegaloid features, no androgynism
Muscle weakness	Distal dominant	No	No	Generalized	Distal dominant
Muscle mounding	Positive	NA	NA	Positive	Positive
Other muscle symptoms	Muscle hypertrophy	Myalgia, muscle stiffness	NA	Muscle hypertrophy	Muscle hypertrophy
Cardiac symptoms	Arrhythmia	No	No	Atrial fibrillation	No
Skeletal abnormalities	Lordosis, Contractures (ankles, shoulders, fingers)	No	No	Scoliosis, contractures (ankles)	Scoliosis
Other symptoms	Constipation	Transient IgA deficiency, recurrent pneumonia	Nephrosis	Umbilical prominence, renal stones	Recurrent pneumonia, chalasia, constipation

NA, not available.

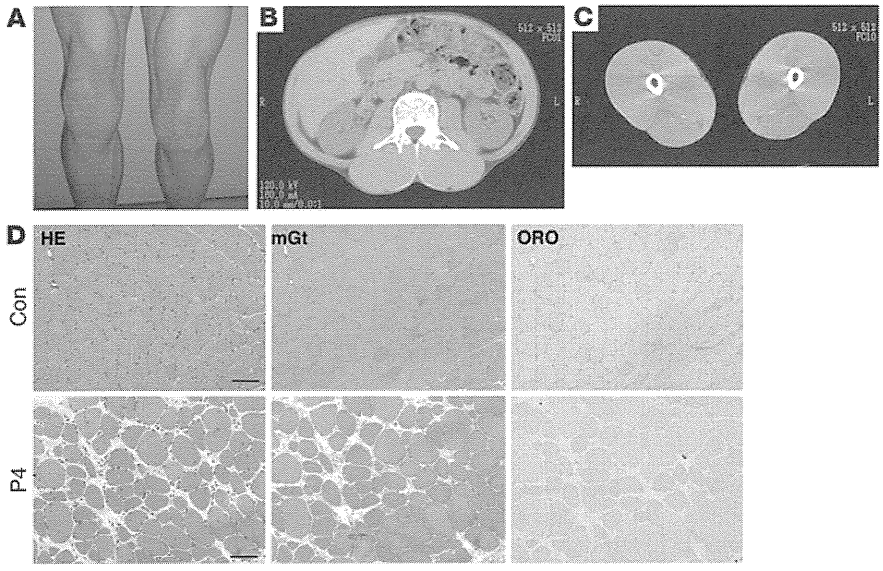

Figure 2
Muscle hypertrophy and dystrophic changes. (**A**) Prominent musculature feature of legs in P5. (**B** and **C**) CT images from P4 showed hypertrophy of paravertebral and thigh muscles with minimal subcutaneous and intra-abdominal fat tissue. (**D**) H&E stain of biopsied skeletal muscle from P4 showed dystrophic changes, including marked variation in fiber size, enlarged fibers with internalized nuclei, endomysial fibrosis, and few necrotic and regenerating fibers. Intramuscular lipid droplets were not increased compared with control. mGt, modified Gomori trichrome; ORO, oil red O. Scale bars: 50 μm.

caused by *CAV3* mutations (data not shown). Similarly, dysferlin was decreased in the sarcolemma and mislocalized into the cytoplasm (data not shown), and the same pattern is also seen in muscles of individuals with *CAV3* mutations (8). Immunoreactivity to caveolin-1 and caveolin-2 in blood vessels was barely detectable in P1–P5 (Figure 3A). Other antibodies related to muscular dystrophy, including dystrophin, sarcoglycans, dystroglycans, emerin, merosin, and collagen VI, showed normal immunostaining patterns (data not shown).

Immunoblotting showed detection of PTRF as an approximately 50-kDa band in control muscles and 3T3 cells, which were used as a positive control. No band was detected in the muscle of P1–P5 (Figure 3B). Caveolin-3 was detected in all samples examined, but relative protein amount, determined using densitometry and normalized by myosin heavy chain (MHC), decreased in P1–P5 compared with control subjects (Figure 3C). The band for caveolin-2 was observed in control muscles and 3T3 cells, but was barely detectable in the muscles of P1–P5 (Figure 3B).

In order to determine mRNA expression of PTRF, RT-PCR was performed using total RNA extracted from biopsied skeletal muscles. Using primers designed to amplify whole coding region of mRNA, PTRF was amplified as a single transcript in control muscles. In contrast, no PCR product was amplified in P1–P5 (Figure 4A). To compare mRNA levels for caveolins, we performed quantitative RT-PCR and normalized results to GAPDH expression. The mRNA amounts of all 3 caveolin families in the patients' muscles were variable, but not markedly decreased, compared with control muscles (Figure 4, B and C). Preserved mRNA levels, but decreased protein amounts of caveolins, suggested destabilization of caveolin proteins when PTRF is lacking, as previously reported (9).

Loss of PTRF causes reduced caveolae formation in human muscles. Greatly reduced caveolae formation was previously reported in PTRF knockdown mammalian cells, zebrafish, and knockout mice (5, 9). Decreased caveolae number was also reported in skeletal muscle from limb girdle muscular dystrophy type 1C (LGMD1C) patients with *CAV3* mutations (10). We therefore examined muscle caveolae in P2 and P3 using electron microscopy. Plasma membrane of muscle fibers from both patients was nearly flat, and caveolae density was notably reduced, compared with control muscle (Figure 5). Caveolae formation in the intramuscular vascular smooth muscle cells was also remarkably reduced (data not shown).

Altered localization of mutant PTRF and reduced interaction with caveolins in transfected cells. In order to determine the intracellular localization of mutant PTRF, FLAG-tagged WT or 2 mutants (c.525delG and c.696_697insC) and T7-tagged caveolin-3 or -1 were cotransfected in C2C12 myoblasts and COS-7 cells. In C2C12 cells, WT PTRF was detected at the cell membrane and colocalized with caveolin-3 (Figure 6A). Interestingly, c.525delG was detected as intranuclear aggregations and was not observed at the cell membrane (Figure 6, A and B). Caveolin-3 was present only in cytoplasm, and did not merge with PTRF (Figure 6A). The c.696_697insC mutant was observed as microtubular filament network in cytoplasm and colocalized with β-tubulin (Figure 6B). This finding is consistent with the localization of the truncated $PTRF_{1-322}$, as described previously (9). Similar mislocalization and/or aggregation of transfected mutant PTRF was observed in COS-7 cells (data not shown).

Table 3
Laboratory data

Measurement	Reference range	P1	P2	P3	P4	P5
CK (IU/l)	56–244	1,374	542–2,253	2,000	554–1,545	645–2,630
Fasting glucose (mg/dl)	70–109	75	99	NA	93–116	102
HbA1c (%)	4.3–5.8	NA	NA	NA	5.0–5.4	NA
Total cholesterol (mg/dl)	130–220	164	NA	NA	185–267	218
Triglyceride (mg/dl)	50–150	93	NA	NA	143–450	359
LDL-C (mg/dl)	70–139	NA	NA	NA	188	NA
Leptin (ng/ml)	0.9–13.0	NA	NA	NA	0.6	NA
Adiponectin (μg/ml)	None	NA	NA	NA	1.05	NA

NA, not available.

Table 4
Oral glucose tolerance test of P1, P2, and P4

	Pre	30 min	60 min	120 min
P1				
Glucose (mg/dl)	75	98	69	62
IRI (μU/ml)	22.8	141.6	64.7	23.8
P2				
Glucose (mg/dl)	99	127	160	172
IRI (μU/ml)	20	53	65	80
P4				
Glucose (mg/dl)	93	124	140	70
CPR (ng/ml)[A]	2.8	5.9	8.3	5.5
IRI (μU/ml)	1.0	22.3	32.9	6.2

IRI, immunoreactive insulin; CPR, C-peptide immunoreactivity. [A]Reference range, 0.7–2.2 ng/ml.

We performed immunoprecipitation assay in order to examine the binding ability of PTRF and caveolins. WT PTRF was coimmunoprecipitated by anti-T7 antibody, and vice versa (Figure 6, C and D). The c.525delG mutant showed smaller molecular weight (estimated 30 kDa; Figure 1B), and no immunoprecipitated protein was detected by FLAG and T7 antibodies. The c.696_697insC mutant showed slightly larger molecular weight, and coimmunoprecipitated proteins were greatly reduced (Figure 6, C and D). These results suggest that mutant PTRFs cannot localize properly and lose their binding ability to caveolins even if they are produced.

Activation of myostatin and Akt signaling pathways in PTRF-deficient skeletal muscles. Caveolin-3 is suggested to have an important role for suppression of myostatin-mediated signaling in skeletal muscle (11). In order to determine the functions of mislocalized caveolin-3 in *PTRF* mutated cells, we performed quantitative RT-PCR for myostatin and immunoblotting analysis to examine phosphorylation status of Mad homolog 2/3 (p-Smad2/3), an intracellular effector of myostatin in skeletal muscles. In P1–P5, increased amounts of p-Smad2/3$^{S423/425}$ were observed in skeletal muscles, while myostatin mRNA levels were variable (Figure 7, A–C). Positive immunoreaction to p-Smad2/3 was detected in few myonuclei from muscle of patients with *PTRF* or *CAV3* mutations, but not in those from muscle of control subjects (data not shown). These results suggest that myostatin signaling is also activated in P1–P5.

Despite the activation of myostatin, a negative regulator of muscle growth, the patients showed hypertrophy of muscles. Since Akt (also known as protein kinase B) is known as the key molecule to regulate muscle mass (12), we examined p-Akt^{T308} and p-Akt^{S473} by immunoblotting analysis. p-Akt was elevated in the muscle of P1–P5 compared with controls, except for p-Akt^{S473} in P2 (Figure 7, D–F). This result suggests that Akt pathway is activated, probably through an as-yet-unidentified mechanism, and could contribute to the muscle hypertrophy observed in P1–P5.

Neuronal NOS activity is variable and mildly increased in PTRF-deficient skeletal muscles. Caveolin-3 is known to interact with and negatively regulate the catalytic activity of neuronal NOS (nNOS) in skeletal muscle (13); this notion is supported by the finding of increased nNOS activity in muscle of transgenic mice expressing mutant caveolin-3 (14). We thus examined nNOS expression and its activity in muscles from patients with mutations in *PTRF* or *CAV3* compared with those from age-matched controls. The immunoreactivity of nNOS was seen in sarcolemma and cytoplasm of each muscle fiber with variable intensity, but no obvious difference was seen between patients and controls (Figure 3A). Immunoblotting analysis also revealed comparable amounts of nNOS (Figure 3, B and D). In order to examine nNOS activity of each muscle fiber, we performed NADPH diaphorase (NDP) activity assay. The intensity of NDP staining appeared variable among muscle fibers and was slightly increased in patients with mutations in *PTRF* or *CAV3* compared with age-matched controls (Figure 8).

Discussion

Lipodystrophy is a heterogeneous group of disorders characterized by loss of adipose tissue from the body. The degree of fat loss varies from small areas to near-complete absence of adipose tissue. The extent of fat loss usually determines clinical severity and metabolic complications, such as insulin resistance and high levels of serum triglycerides.

Several genes responsible for inherited lipodystrophy have been identified. CGL is an autosomal-recessive disorder, with most patients presenting soon after birth with severe insulin resistance and elevated serum triglycerides. CGL1 is caused by mutations in *AGPAT2* on chromosome 9q34, which encodes 1-acylglycerol-3-phospate-O-acyltransferase 2, an enzyme involved in the biosynthesis of triacylglycerol and glycerophospholipids (15). CGL2 is caused by mutations in *BSCL2* on chromosome 11q13, which encodes a functionally unknown protein named seipin (16). Recently, mutations in *CAV1* on chromosome 7q31 have been reported to cause generalized (i.e., CGL3) and partial lipodystrophy (17, 18).

Several causative genes for autosomal-dominant familial partial lipodystrophy are known: *LMNA* on chromosome 1q21 (19), *ZMPSTE24* on chromosome 1p34 (20), *AKT2* on chromosome 19q13 (21), *PPARG* on chromosome 3p25 (22), and *LMNB2* on chromosome 19q1 (23). Nevertheless, many patients clinically diagnosed with lipodystrophy carry no mutation in the known genes, suggesting the presence of other causative genes.

Here we conclude that *PTRF* mutations can cause CGL. In our series, patients showed generalized loss of adipose tissue from infancy or early childhood. Because PTRF is reported to colocalize with hormone-sensitive lipase and translocate to the nucleus in the presence of insulin in adipocytes (24), it could be surmised that PTRF plays an important role in lipid metabolism and insulin-regulated gene expression. Interestingly, metabolic complications were milder in patients with *PTRF* mutations than in patients with CGL1 and CGL2, and these were observed only in the elder patients. Although we could not examine the status of caveolae and caveolins in adipose tissues, the secondary deficiency of caveolins might have an important role in the process of lipodystrophy, since *CAV1* mutation can cause lipodystrophy in both humans and mice (17, 18, 25). Notably, the heterozygous parents had mild metabolic disorders, but a robust conclusion could not be reached, as a limited number of the heterozygous carriers of the *PTRF* mutation were available to us. Further investigation is needed to determine the effect of haploinsufficiency of PTRF.

Skeletal muscle symptoms with serum CK elevation represent another common symptom in patients with *PTRF* mutations. The clinical and pathological findings are very similar to those observed in patients with *CAV3* mutation (7, 26–28), although P1–P5 had no *CAV3* mutations. The secondary loss of caveolin-3 in the sarcolemma may contribute to the muscle phenotype. Moreover, serum CK elevation may be a good laboratory marker for diagnosis of lipodystrophy patients with *PTRF* mutations.

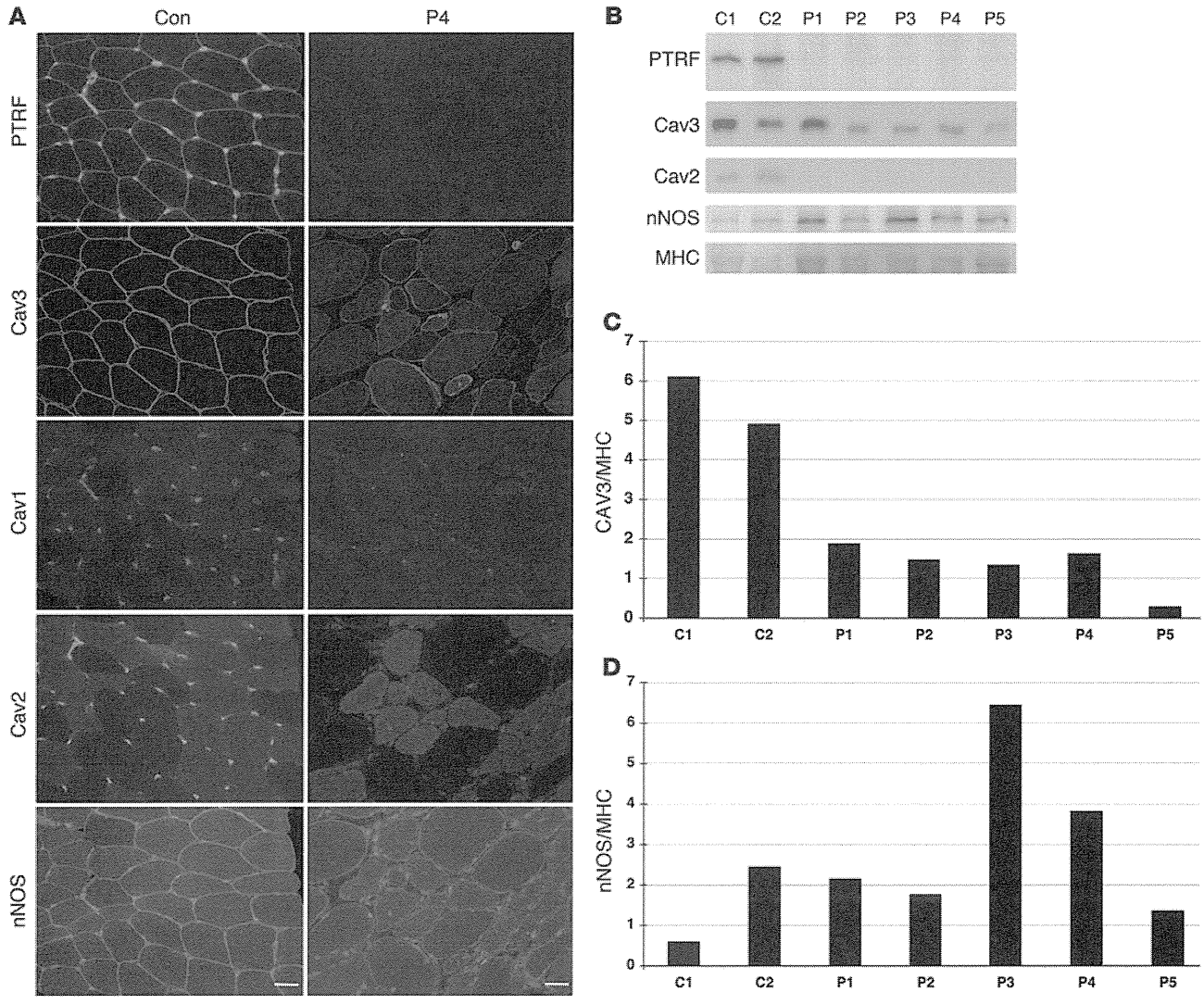

Figure 3

Loss of PTRF is associated with deficiency and mislocalization of caveolins in muscle. (**A**) In control muscle, PTRF was clearly seen in sarcolemma as strongly staining blood vessels. Caveolin-3 (Cav3) was clearly visible at sarcolemma, and caveion-1 and -2 stained intramuscular blood vessels. The muscle of P4 was negative for PTRF. Membrane staining of caveolin-3 was reduced with increased cytoplasmic staining, and caveolin-1 and -2 were barely detectable. Immunoreactivity of nNOS varied between muscle fibers, but was not markedly different between control and patient muscle. Scale bar: 50 μm. (**B**) Immunoblotting analysis of skeletal muscles. 3T3 cells were used as a positive control. PTRF and caveolin-2 were seen only in the muscles of 2 control subjects and in 3T3 cells, and were barely detectable in the muscles of P1–P5. The bands for caveolin-3 and nNOS were variably seen. (**C** and **D**) Quantification of immunoreactive bands was performed by densitometric analysis and normalized with MHC. In P1–P5, relative amounts of caveolin-3 decreased compared with control subjects (**C**), whereas nNOS amounts varied (**D**).

Caveolin-3 was previously reported to have an important role in inhibition of myostatin signaling by suppressing activation of its type I receptor. In mutant *Cav3* transgenic mice, loss of caveolin-3 causes muscular atrophy with increased p-Smad2, and this muscle atrophy can be rescued by myostatin inhibition (11). Consistent with the secondary reduction of caveolin-3, skeletal muscles from P1–P5 showed increased amounts of p-Smad2/3. Unexpectedly, however, muscle hypertrophy was seen in these patients.

The Akt pathway, when activated, is known to promote protein synthesis, stimulate muscle hypertrophy, and inhibit atrophy-related gene expression by phosphorylating FoxO transcription factors (12). This pathway is also known to play a pivotal role in the regulation of glucose transport and glycogen synthesis in skeletal muscle cells. Akt is activated by insulin, various growth factors, nutrients, and exercise, whereas it is negatively regulated by myostatin and cytokines. Akt is phosphorylated at T308 by phosphoinositide-dependent kinase and at S473 by mammalian target of rapamycin in association with rictor. The increase in phosphorylated Akt in the muscle of P1–P5 may explain, at least in part, the muscle hypertrophy observed. Akt pathway activation might be associated with the metabolic complications observed in P1–P5. However, the upregulation of myostatin observed is contradictory to the established knowledge on muscle hypertrophy. This would be worthwhile to investigate in future studies, in order to

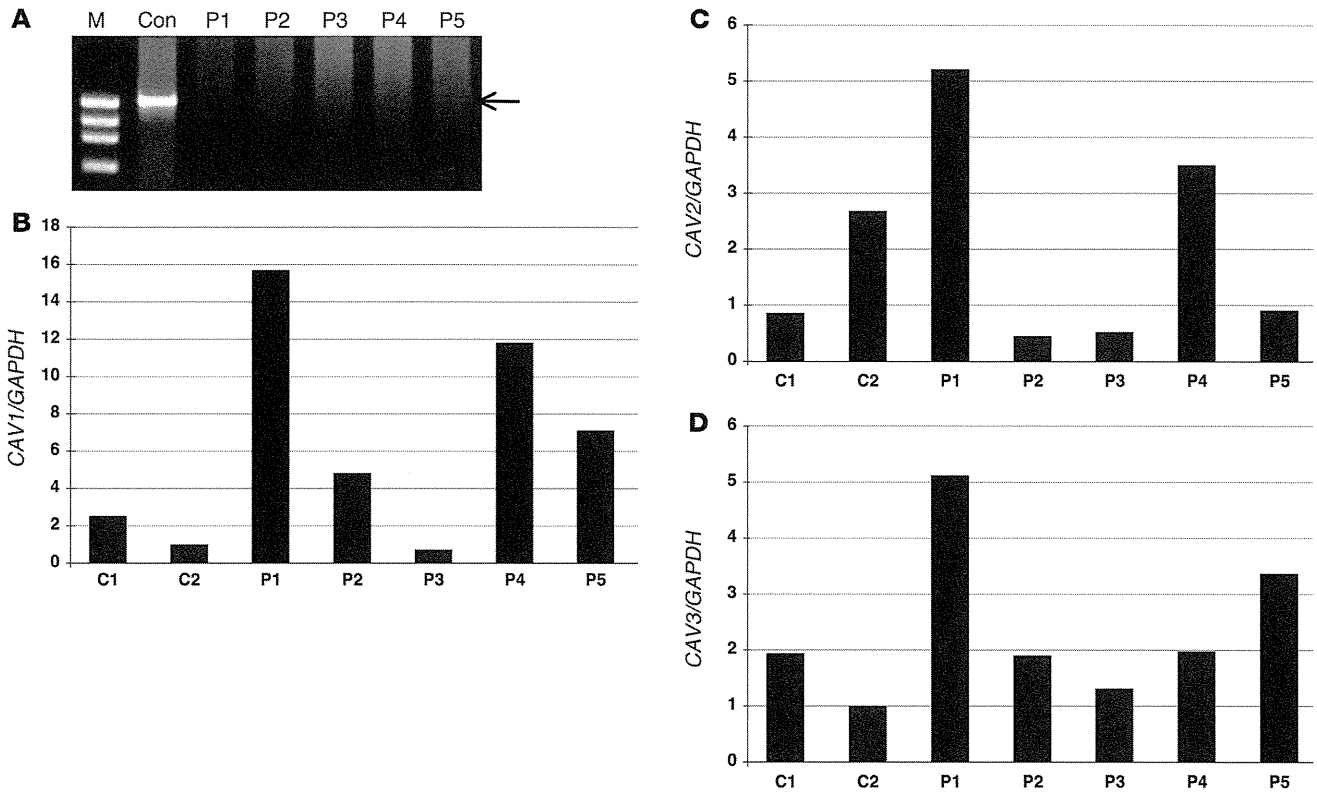

Figure 4
mRNA expression of PTRF in skeletal muscle, and quantitative RT-PCR of mRNAs for caveolins. (**A**) RT-PCR analysis revealed a single band for *PTRF* mRNA (arrow) in a control subject, but no detectable product was seen in P1–P5. M, marker. (**B–D**) By quantitative RT-PCR, mRNA for *CAV1*, *CAV2*, and *CAV3* normalized with *GAPDH* expression was not decreased in P1–P5.

elucidate the role of PTRF deficiency in muscle hypertrophy and related signaling pathway.

In addition to lipodystrophy and muscular dystrophy, P1–P5 had various other symptoms, whose association to *PTRF* mutation might be difficult to ascertain at this time. For example, 2 of 5 patients had arrhythmia. Although we could not examine the expression of caveolins in cardiac muscle, this cardiac abnormality may be caused by secondary deficiency of caveolins in heart, as cardiac involvement was previously reported in patients with *CAV3* mutations and in mutant mice with double knockout of *Cav1* and *Cav3* (29–33).

Remarkable reduction in expression of caveolin-1 and -2 with decreased caveolae density was observed in vascular endothelial cells in P1–P5. There was no obvious symptom related to vascular endothelial blood vessels in the patients; however, further careful investigation is necessary in order to determine the involvement of endothelial cells, which was observed in *Cav1* knockout mice (34). The severe constipation and esophageal dilatation observed in the patients might be associated with dysfunction of caveolin-1 in smooth muscle cells, as *Cav1* knockout mice had alteration of smooth muscles and interstitial cells of Cajal, the pacemaker cells of the muscle layers of the gastrointestinal tract (35).

Caveolae was previously suggested to have a role in the internalization of growth hormone in vitro (36). The acromegaloid features, accelerated bone age, or abnormal growth hormone activity observed in 3 patients in the present study might be associated with reduced caveolae formation. Recurrent pneumonia and transient immunodeficiency observed in 2 patients were also noted, although the pathomechanisms are still unknown. Further detailed studies are needed to elucidate the roles of PTRF; however,

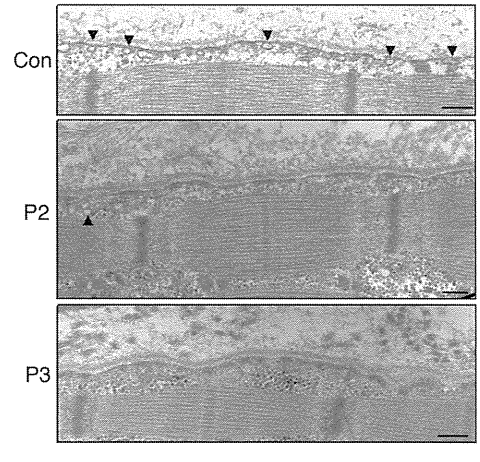

Figure 5
Reduced caveolae formation in skeletal muscle, as assessed by electron microscopy. In control muscle, an abundance of caveolae (arrowheads) was observed close to the plasma membrane. Plasma membrane of muscle fibers from P2 and P3 was nearly flat, and caveolae density was greatly reduced compared with that of control muscle. Only a few caveolae were seen in P2. Scale bars: 200 nm.

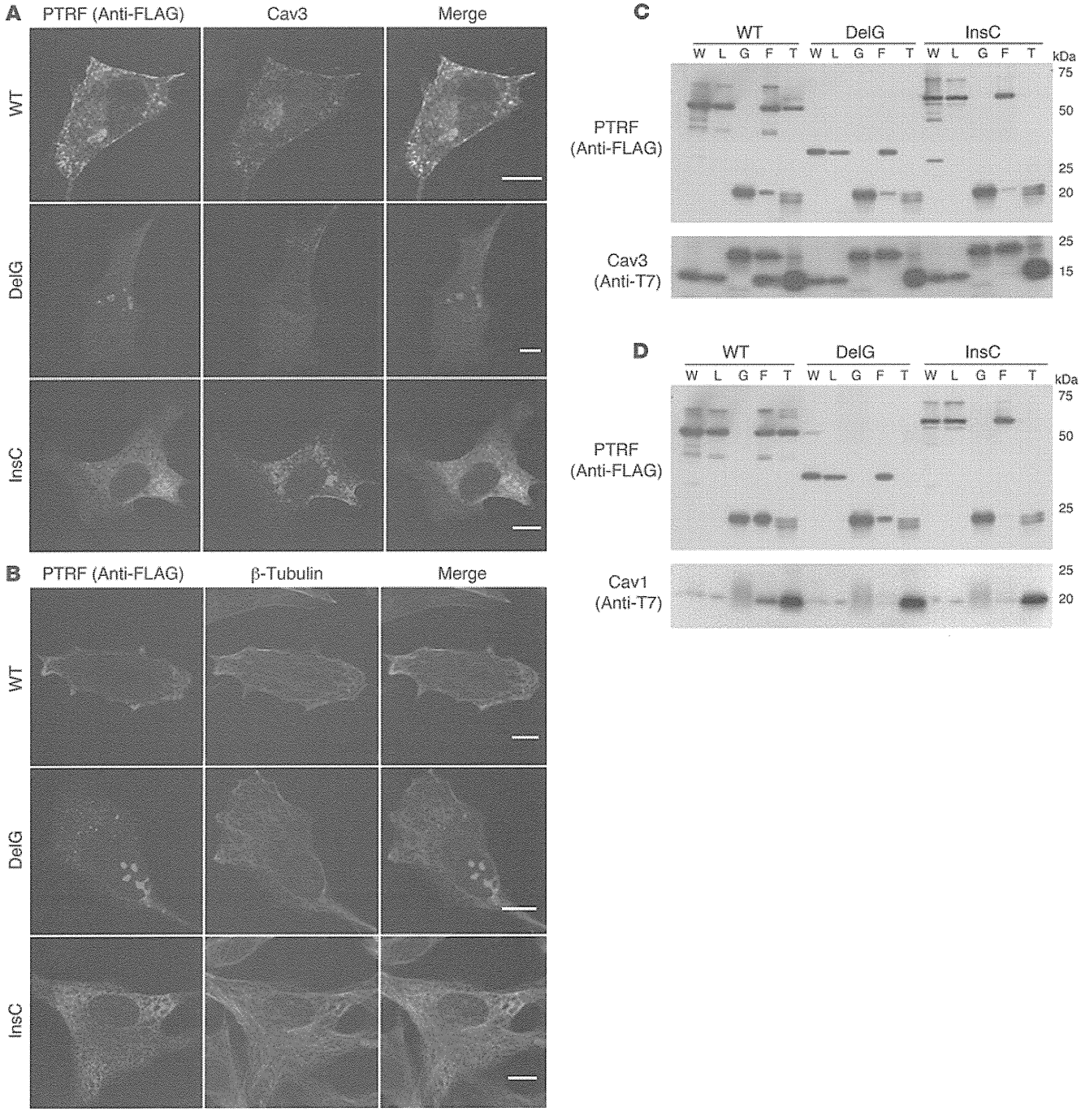

Figure 6

Altered localization of mutant PTRF in C2C12 cells and reduced binding ability to caveolins. C2C12 myoblasts were cotransfected with FLAG-tagged WT or mutant (c.525delG or c.696_697insC) PTRF cDNA and T7-tagged human caveolin-3. (**A** and **B**) WT PTRF stained by anti-FLAG antibody colocalized with caveolin-3 at the cell membrane. The deletion mutant accumulated in the nucleus, and the insertion mutant was seen in cytoplasm. (**A**) Membrane staining of caveolin-3 was decreased and was not colocalized with mutant PTRF. (**B**) The PTRF insertion mutant clearly colocalized with β-tubulin. Scale bars: 10 μm. (**C** and **D**) COS-7 cells were cotransfected with FLAG-tagged WT or mutant PTRF cDNA and T7-tagged human caveolin-3 (**C**) or caveolin-1 (**D**). The PTRF deletion mutant showed smaller molecular weight (estimated 30 kDa), and no immunoprecipitated protein was detected for FLAG or T7 antibodies. The PTRF insertion mutant showed slightly larger molecular weight, and amounts of coimmunoprecipitated proteins were greatly reduced. W, whole homogenate; L, cell lysate, G, control IgG; F, anti-FLAG; T, anti-T7.

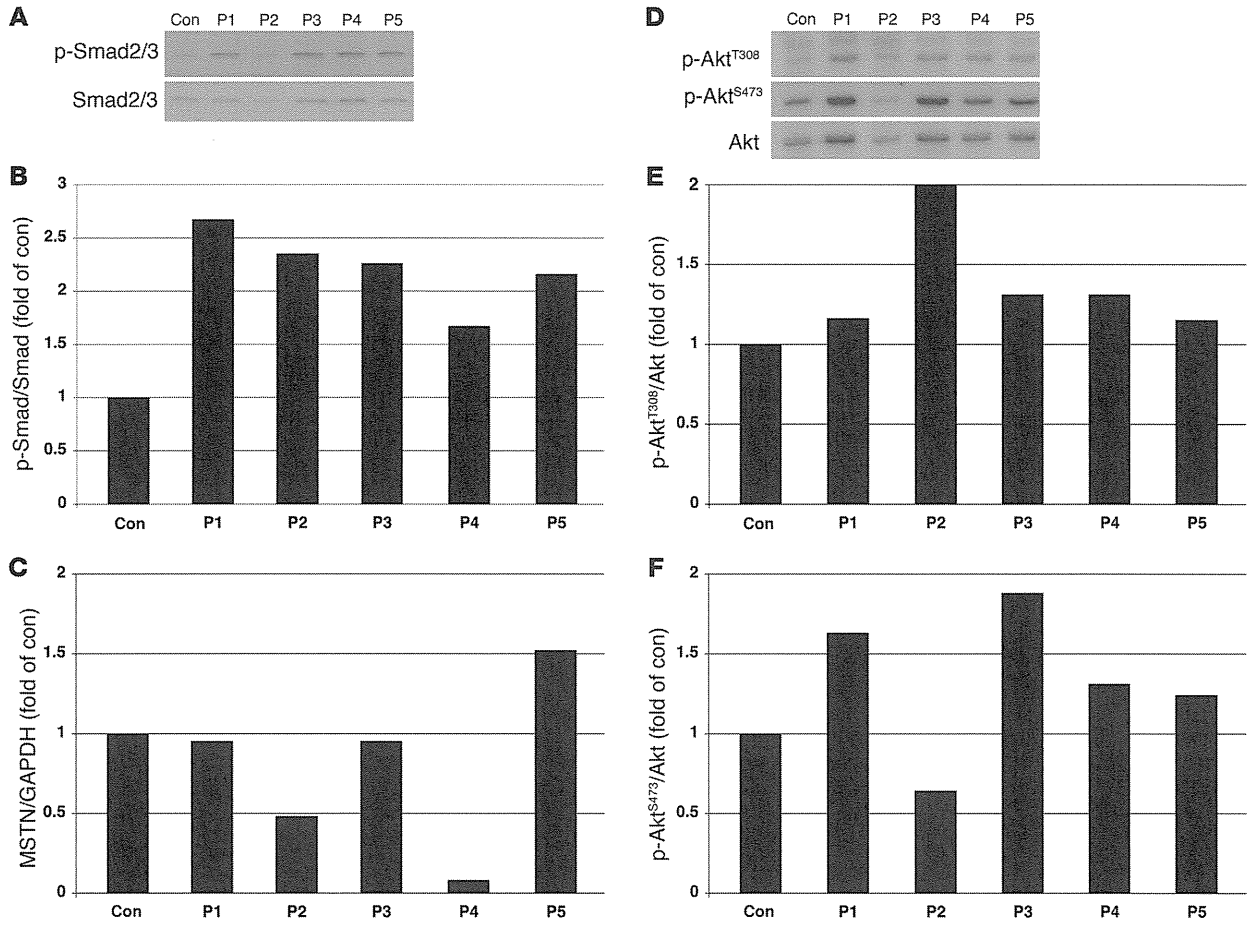

Figure 7

Increased p-Smad2 and p-Akt in P1–P5 skeletal muscle. (**A–C**) Immunoblotting analysis of Smad2/3 and p-Smad2/3$^{S423/425}$ (**A**) and densitometric analysis (**B**) showed increased p-Smad2/3 in P1–P5 compared with control muscle, with variable mRNA expression levels of myostatin (MSTN; **C**). (**D–F**) Immunoblotting analysis of p-Akt^{T308} and p-Akt^{S473}. Total Akt (**D**) and densitometric analysis (**E** and **F**) showed increased amounts of p-Akt in all patients except for p-Akt^{S473} in P2.

most clinical features observed in P1–P5 are likely to be explained by secondary reduction of caveolae and deficiency of caveolins.

Previously, Rajab et al. reported 10 of 17 patients with congenital generalized lipodystrophy unlinked to the loci of known CGL genes (37). The patients showed reduced exercise tolerance, percussion myoedema, cardiac hypertrophy, and arrhythmias. None of these patients had insulin resistance or early endocrine abnormalities (37). Ghanem also reported myoedema in a patient with Berardinelli-Seip lipodystrophy (38). Very recently, Simha et al. described CGL patients with muscle weakness and cervical spine instability (39). Because muscle involvement of these patients is similar to that of P1–P5 in the present study, *PTRF* mutations may not be rare in CGL patients.

This entity of generalized lipodystrophy with muscular dystrophy — which we believe to be novel — seems to represent a complicated disorder, as the occurrence of other symptoms could not readily be explained. Collection of detailed clinical information would therefore be essential in order to understand the precise function of PTRF.

Methods

Clinical materials. All clinical materials used in this study were obtained for diagnostic purposes and with informed consent. Subjects were selected from 2,745 muscular dystrophy specimens kept in the muscle repository of the National Center of Neurology and Psychiatry. The present studies were approved by the Ethical Committee at National Center of Neurology and Psychiatry.

Mutation screening and haplotype analysis. Genomic DNA was isolated from peripheral lymphocytes or muscles using standard techniques. All exons and their flanking intronic regions of *PTRF*, *CAV3*, *LMNA*, *AGPAT2*, *BSCL2*, *CAV1*, *PPARG*, *AKT2*, and *ZMPSTE24* were directly sequenced using genomic DNA from all patients using an ABI PRISM 3100 automated sequencer (Applied Biosystems). Primer sequences are listed in Supplemental Table 3. To confirm the compound heterozygosity in P5, the PCR product was cloned and sequenced. In order to determine the frequency of the mutations in *PTRF*, we performed enzyme digestion of PCR products from 200 Japanese control subjects using *Hpy*188III (New England Biolabs) for c.696_697insC and *Taq*I (New England Biolabs) for c.525delG. *Mbo*II (New England Biolabs) was used for enzyme digestion of PCR products to detect the c.1138G>A substitution in *BSCL2*.

For haplotype analysis, we used 6 SNPs (rs2062213, rs8070945, rs963988, rs963987, rs963986, and rs9252) within *PTRF*. PCR products were analyzed by direct sequencing or enzyme digestion using *Mae*III (Boehringer Mannheim). We also identified a novel 9-bp insertion polymorphism at the

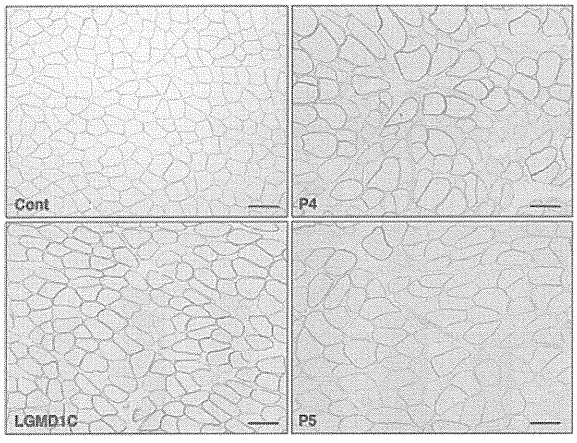

Figure 8
NDP activity assay. NDP activity was variable between muscle fibers, and was slightly increased in the muscle of P4, P5, and a LGMD1C patient with *CAV3* mutation compared with an age-matched control subject. Scale bars: 100 μm.

3′ noncoding region, and its frequency was calculated by PCR amplification using 50 Japanese control individuals. We also examined 2 microsatellite markers, STS-W93348 and D17S1185, the closest markers to *PTRF*. PCR product size was analyzed by GeneMapper using ABI 310 automated sequencer (Applied Biosystems).

Histochemical analysis. Biopsied muscle specimens were flash frozen with isopentane cooled in liquid nitrogen. Serial 10-μm-thick frozen sections were analyzed with 20 kinds of histochemical staining, including H&E, modified Gomori trichrome, NADH-tetrazolium reductase, and oil red O. The NDP activity assay was performed to examine nNOS activity of each muscle fiber, as described previously (40). In brief, 10-μm-thick frozen sections were fixed with 4% paraformaldehyde in PBS for 2 hours at 4°C. After a brief rinse with PBS, sections were incubated with 0.2% Triton X-100 in PBS for 20 minutes at 37°C. The reaction was performed for 1 hour in a dark, humidified chamber at 37°C in 0.2% Triton X-100, 0.2 mM NADPH, and 0.16 mg/ml nitro blue tetrazolium. The reaction was terminated by washing with water. We examined 6 age-matched controls and 2 LGMD1C patients with *CAV3* mutations (p.R27G and p.E33K).

Immunohistochemical analysis. Immunostaining was performed using standard methods. Serial 6-μm-thick frozen muscle sections were fixed in cold acetone for 5 minutes. After blocking with normal goat serum, sections were incubated with the primary antibodies for 2 hours at 37°C. We used antibodies against PTRF (A301-269A and A301-271A; BETHYL Laboratories), caveolin-1 (BD Biosciences), caveolin-2 (Sigma-Aldrich), caveolin-3 (BD Biosciences), and nNOS (BD Biosciences). Rabbit anti-PTRF antibody of A301-269A recognizes residue from 125 to 175, and A301-271A was raised against residue 238 and 288 of human PTRF (Figure 1B). In order to exclude other diagnosable muscular dystrophies, we used antibodies for dystrophin (DYS1, DYS2, and DYS3; Novocastra); α-, β-, γ-, and δ-sarcoglycans (Novocastra); α-dystroglycan (Upstate Biotech); β-dystroglycan (Novocastra); dysferlin (Novocastra); emerin (Novocastra); merosin (Chemicon); and collagen VI (ICN Biomedicals). After 6 rinses with PBS, sections were incubated with secondary antibodies of Alexa Fluor 488– or Alexa Fluor 568–labeled goat anti-mouse or -rabbit antibodies at room temperature for 45 minutes.

Immunoblotting analysis. Immunoblotting analysis was performed according to standard methods. Frozen muscle specimens were homogenized in SDS sample buffer and centrifuged at 15,000 *g* for 5 minutes. Protein (20 μg) from each sample was loaded on 12% SDS-polyacrylamide gels and transferred to PVDF membranes (Millipore). The membranes were blocked with 5% skim milk in PBS and immunoreacted with antibodies to PTRF (A301-269A and A301-271A), caveolin-2, caveolin-3, nNOS, Smad2/3 (Cell Signaling Technology), p-Smad2/3$^{S423/425}$ (Santa Cruz Biotechnology Inc.), Akt (Cell Signaling Technology), p-Akt^{T308} (Cell Signaling Technology), and p-Akt^{S473} (Cell Signaling Technology) overnight at 4°C. After washing in PBS containing 0.1% Tween-20, the membrane was incubated with horseradish peroxidase–labeled secondary antibody and visualized with ECL (Amersham Pharmacia Biotech). Data were analyzed using LAS-1000 chemiluminescence imaging system (Fujifilm). Quantification of immunoreactive bands was performed by densitometric analysis using Quantity One (PDI), and protein amounts for caveolin-3 and nNOS were normalized by the intensity of MHC. The ratio of p-Smad2/3 and p-Akt, to Smad and Akt, respectively, was also calculated.

Electron microscopy. Muscle specimens were fixed with 2% glutaraldehyde in 0.1 M cacodylate buffer. After shaking with a mixture of 4% osmium tetroxide, 1.5% lanthanum nitrate, and 0.2 M s-collidine for 2–3 hours, samples were embedded in epoxy resin. Semithin sections (1 μm thick) were stained with toluidine blue. Ultrathin sections 50 nm thick were stained with uranyl acetate and lead citrate, then examined under H-600 transmission electron microscope (Hitachi) at 75 kV.

RT-PCR. Total RNA was extracted from biopsied skeletal muscles using TRIzol (Invitrogen), and RT-PCR was performed using SuperScript III (Invitrogen) with random hexamer according to the manufacturer's instructions. Primers for each gene were located on different exons or directly spanning exon-exon boundaries of the genomic sequence in order to minimize amplification from any contaminating genomic DNA. After performing preliminary gradient PCR assays, the optimal annealing temperature for all the primer pairs was determined in order to generate the lowest Ct value as well as a sharp melting peak, with no amplification of nonspecific products or primer-dimer artifacts. Quantitative RT-PCR was performed to compare the mRNA expression of caveoin-1, caveolin-2, caveolin-3, and myostatin using Rotor-Gene 6000 according to the manufacturer's instructions (Corbett Life Science). The reactions were performed in reference to the GAPDH. We used 4 points consisting of 10-fold serial dilution using each primer set to build the standard curve. The PCR reaction (50 cycles) was followed by a melting curve analysis, ranging from 72°C to 95°C, with temperature increasing steps of 0.5°C every 10 seconds. Baseline and threshold values were automatically determined and analyzed. R^2 values exceeded 0.97. The 2–standard curve method was used to determine the relative expression ratio of the target gene in the patient samples versus the control sample, with reference to GAPDH expression.

Cell culture and transfection. COS-7 and C2C12 cells were maintained at 37°C in a humidified atmosphere of 5% CO_2 in DMEM (Sigma-Aldrich) supplemented with 10% fetal bovine serum. Full-length PTRF and caveolin-1 and -3 were amplified using total RNA from control human muscle and cloned into the pGEM-T-easy vector (Promega). The PTRF mutants c.525delG and c.696_697insC were generated using appropriate primers. All primer sequences are shown in Supplemental Table 3.

Immunocytochemistry. COS-7 and C2C12 myoblasts were cotransfected with FLAG-tagged WT or mutant (c.525delG or c.696_697insC) PTRF cDNA and T7-tagged human caveolin-3 using FuGENE6 (Roche). Transfectants were fixed for 30 minutes in 2% paraformaldehyde or 100% methanol, then permeabilized in 0.1% Triton X-100 for 10 minutes. Polyclonal antibodies to FLAG (Sigma-Aldrich) with caveolin-3 (BD Biosciences) or FLAG with β-tubulin (Calbiochem) were applied for double staining.

Immunoprecipitation. COS-7 cells were cotransfected with FLAG-tagged WT or mutant (c.525delG or c.696_697insC) PTRF cDNA and T7-tagged human caveolin-1 or caveolin-3 using FuGENE6 (Roche). The sequences of all constructs were verified with DNA sequencing using ABI PRISM 310 (Applied Biosystems). After 48 hours, the lysates from transfectants were

solubilized with 50 mM Tris-HCl (pH 7.5), 150 mM NaCl, 50 mM EDTA, 1% Triton X-100, and Complete-mini EDTA-free proteinase inhibitors (Roche) (9). The solubilized lysate precleared with Protein G Sepharose (GE Healthcare) was incubated with anti-FLAG (M2; Sigma-Aldrich) and anti-T7 (Novagen) antibodies. Immunoprecipitated proteins were dissociated from beads by boiling in sample buffer and were resolved by SDS-PAGE. Immunoblotting was performed using standard techniques.

Acknowledgments

We thank Sherine Shalaby (Heliopolis Neurocenter, Cairo, Egypt) and May Malicdan (National Center of Neurology and Psychiatry) for reviewing the manuscript. This study was supported by "Research on Psychiatric and Neurological Diseases and Mental Health" of "Health Labour Sciences Research Grant" and by "Research Grant (20B-12, 20B-13) for Nervous and Mental Disorders" from the Ministry of Health, Labor, and Welfare of Japan; by grants from the Human Frontier Science Program; by a Grant-in-Aid for Scientific Research from Japan Society for the Promotion of Science; by Research on Publicly Essential Drugs and Medical Devices from the Japanese Health Sciences Foundation; and by the Program for Promotion of Fundamental Studies in Health Sciences of the National Institute of Biomedical Innovation (NIBIO).

Received for publication January 20, 2009, and accepted in revised form June 3, 2009.

Address correspondence to: Yukiko K. Hayashi, Department of Neuromuscular Research, National Institute of Neuroscience, National Center of Neurology and Psychiatry, 4-1-1 Ogawa-higashi, Kodaira, 187-8502 Tokyo, Japan. Phone: 81-42-341-2711, Fax: 81-42-346-1742; E-mail: hayasi_y@ncnp.go.jp.

1. Scherer, P.E., et al. 1997. Cell-type and tissue-specific expression of caveolin-2. Caveolins 1 and 2 co-localize and form a stable hetero-oligomeric complex in vivo. *J. Biol. Chem.* **272**:29337–29346.
2. Tang, Z., et al. 1996. Molecular cloning of caveolin-3, a novel member of the caveolin gene family expressed predominantly in muscle. *J. Biol. Chem.* **271**:2255–2261.
3. Galbiati, F., Razani, B., and Lisanti, M.P. 2001. Emerging themes in lipid rafts and caveolae. *Cell.* **106**:403–411.
4. Thomas, C.M., and Smart, E.J. 2008. Caveolae structure and function. *J. Cell. Mol. Med.* **12**:796–809.
5. Hill, M.M., et al. 2008. PTRF-Cavin, a conserved cytoplasmic protein required for caveola formation and function. *Cell.* **132**:113–124.
6. Liu, L., et al. 2008. Deletion of Cavin/PTRF causes global loss of caveolae, dyslipidemia, and glucose intolerance. *Cell Metab.* **8**:310–317.
7. Minetti, C., et al. 1998. Mutations in the caveolin-3 gene cause autosomal dominant limb-girdle muscular dystrophy. *Nat. Genet.* **18**:365–368.
8. Matsuda, C., et al. 2001. The sarcolemmal proteins dysferlin and caveolin-3 interact in skeletal muscle. *Hum. Mol. Genet.* **10**:1761–1766.
9. Liu, L., and Pilch, P.F. 2008. A critical role of cavin (polymerase I and transcript release factor) in caveolae formation and organization. *J. Biol. Chem.* **283**:4314–4322.
10. Minetti, C., et al. 2002. Impairment of caveolae formation and T-system disorganization in human muscular dystrophy with caveolin-3 deficiency. *Am. J. Pathol.* **160**:265–270.
11. Ohsawa, Y., et al. 2006. Muscular atrophy of caveolin-3-deficient mice is rescued by myostatin inhibition. *J. Clin. Invest.* **116**:2924–2934.
12. Frost, R.A., and Lang, C.H. 2007. Protein kinase B/Akt: a nexus of growth factor and cytokine signaling in determining muscle mass. *J. Appl. Physiol.* **103**:378–387.
13. Venema, V.J., Ju, H., Zou, R., and Venema, R.C. 1997. Interaction of neuronal nitric-oxide synthase with caveolin-3 in skeletal muscle. Identification of a novel caveolin scaffolding/inhibitory domain. *J. Biol. Chem.* **272**:28187–28190.
14. Sunada, Y., et al. 2001. Transgenic mice expressing mutant caveolin-3 show severe myopathy associated with increased nNOS activity. *Hum. Mol. Genet.* **10**:173–178.
15. Agarwal, A.K., et al. 2002. AGPAT2 is mutated in congenital generalized lipodystrophy linked to chromosome 9q34. *Nat. Genet.* **31**:21–23.
16. Magre, J., et al. 2001. Identification of the gene altered in Berardinelli-Seip congenital lipodystrophy on chromosome 11q13. *Nat. Genet.* **28**:365–370.
17. Kim, C.A., et al. 2008. Association of a homozygous nonsense caveolin-1 mutation with Berardinelli-Seip congenital lipodystrophy. *J. Clin. Endocrinol. Metab.* **93**:1129–1134.
18. Cao, H., Alston, L., Ruschman, J., and Hegele, R.A. 2008. Heterozygous CAV1 frameshift mutations (MIM 601047) in patients with atypical partial lipodystrophy and hypertriglyceridemia. *Lipids Health Dis.* **7**:3.
19. Cao, H., and Hegele, R.A. 2000. Nuclear lamin A/C R482Q mutation in canadian kindreds with Dunnigan-type familial partial lipodystrophy. *Hum. Mol. Genet.* **9**:109–112.
20. Agarwal, A.K., et al. 2003. Phenotypic and genetic heterogeneity in congenital generalized lipodystrophy. *J. Clin. Endocrinol. Metab.* **88**:4840–4847.
21. George, S., et al. 2004. A family with severe insulin resistance and diabetes due to a mutation in AKT2. *Science.* **304**:1325–1328.
22. Barroso, I., et al. 1999. Dominant negative mutations in human PPARgamma associated with severe insulin resistance, diabetes mellitus and hypertension. *Nature.* **402**:880–883.
23. Hegele, R.A., et al. 2006. Sequencing of the reannotated LMNB2 gene reveals novel mutations in patients with acquired partial lipodystrophy. *Am. J. Hum. Genet.* **79**:383–389.
24. Aboulaich, N., Ortegren, U., Vener, A.V., and Stralfors, P. 2006. Association and insulin regulated translocation of hormone-sensitive lipase with PTRF. *Biochem. Biophys. Res. Commun.* **350**:657–661.
25. Razani, B., et al. 2002. Caveolin-1-deficient mice are lean, resistant to diet-induced obesity, and show hypertriglyceridemia with adipocyte abnormalities. *J. Biol. Chem.* **277**:8635–8647.
26. Fulizio, L., et al. 2005. Molecular and muscle pathology in a series of caveolinopathy patients. *Hum. Mutat.* **25**:82–89.
27. Betz, R.C., et al. 2001. Mutations in CAV3 cause mechanical hyperirritability of skeletal muscle in rippling muscle disease. *Nat. Genet.* **28**:218–219.
28. Sugie, K., et al. 2004. Two novel CAV3 gene mutations in Japanese families. *Neuromuscul. Disord.* **14**:810–814.
29. Hayashi, T., et al. 2004. Identification and functional analysis of a caveolin-3 mutation associated with familial hypertrophic cardiomyopathy. *Biochem. Biophys. Res. Commun.* **313**:178–184.
30. Vatta, M., et al. 2006. Mutant caveolin-3 induces persistent late sodium current and is associated with long-QT syndrome. *Circulation.* **114**:2104–2112.
31. Park, D.S., et al. 2002. Caveolin-1/3 double-knockout mice are viable, but lack both muscle and non-muscle caveolae, and develop a severe cardiomyopathic phenotype. *Am. J. Pathol.* **160**:2207–2217.
32. Woodman, S.E., et al. 2002. Caveolin-3 knock-out mice develop a progressive cardiomyopathy and show hyperactivation of the p42/44 MAPK cascade. *J. Biol. Chem.* **277**:38988–38997.
33. Zhao, Y.Y., et al. 2002. Defects in caveolin-1 cause dilated cardiomyopathy and pulmonary hypertension in knockout mice. *Proc. Natl. Acad. Sci. U. S. A.* **99**:11375–11380.
34. Xu, Y., Buikema, H., van Gilst, W.H., and Henning, R.H. 2008. Caveolae and endothelial dysfunction: filling the caves in cardiovascular disease. *Eur. J. Pharmacol.* **585**:256–260.
35. El-Yazbi, A.F., Cho, W.J., Boddy, G., and Daniel, E.E. 2005. Caveolin-1 gene knockout impairs nitrergic function in mouse small intestine. *Br. J. Pharmacol.* **145**:1017–1026.
36. Lobie, P.E., Sadir, R., Graichen, R., Mertani, H.C., and Morel, G. 1999. Caveolar internalization of growth hormone. *Exp. Cell Res.* **246**:47–55.
37. Rajab, A., Heathcote, K., Joshi, S., Jeffery, S., and Patton, M. 2002. Heterogeneity for congenital generalized lipodystrophy in seventeen patients from Oman. *Am. J. Med. Genet.* **110**:219–225.
38. Ghanem, Q. 1993. Percussion myoedema in a Pakistani boy with Berardinelli Seip lipodystrophy syndrome. *Clin. Genet.* **44**:277–278.
39. Simha, V., Agarwal, A.K., Aronin, P.A., Iannaccone, S.T., and Garg, A. 2008. Novel subtype of congenital generalized lipodystrophy associated with muscular weakness and cervical spine instability. *Am J. Med. Genet. A.* **146A**:2318–2326.
40. Kameya, S., et al. 1999. alpha1-syntrophin gene disruption results in the absence of neuronal-type nitric-oxide synthase at the sarcolemma but does not induce muscle degeneration. *J. Biol. Chem.* **274**:2193–2200.

Mitochondrial Lon protease regulates mitochondrial DNA copy number and transcription by selective degradation of mitochondrial transcription factor A (TFAM)

Yuichi Matsushima[a,b], Yu-ichi Goto[b], and Laurie S. Kaguni[a,1]

[a]Department of Biochemistry and Molecular Biology, and Center for Mitochondrial Science and Medicine, Michigan State University, East Lansing, MI 48824-1319; and [b]Department of Mental Retardation and Birth Defect Research, National Institute of Neuroscience, National Center of Neurology and Psychiatry, 4-1-1 Ogawahigashi, Kodaira, Tokyo 187-8502, Japan

Edited* by I. Robert Lehman, Stanford University School of Medicine, Stanford, CA, and approved August 25, 2010 (received for review June 23, 2010)

Lon is the major protease in the mitochondrial matrix in eukaryotes, and is well conserved among species. Although a role for Lon in mitochondrial biogenesis has been proposed, the mechanistic basis is unclear. Here, we demonstrate a role for Lon in mtDNA metabolism. An RNA interference (RNAi) construct was designed that reduces Lon to less than 10% of its normal level in *Drosophila* Schneider cells. RNAi knockdown of Lon results in increased abundance of mitochondrial transcription factor A (TFAM) and mtDNA copy number. In a corollary manner, overexpression of Lon reduces TFAM levels and mtDNA copy number. Notably, induction of mtDNA depletion in Lon knockdown cells does not result in degradation of TFAM, thereby causing a dramatic increase in the TFAM:mtDNA ratio. The increased TFAM:mtDNA ratio in turn causes inhibition of mitochondrial transcription. We conclude that Lon regulates mitochondrial transcription by stabilizing the mitochondrial TFAM:mtDNA ratio via selective degradation of TFAM.

AAA+ protease | mtDNA maintenance | quality control

Lon is the major protease in the mitochondrial matrix and is well conserved among species (1–4). Lon is a member of the super family of ATPases associated with diverse cellular activities (AAA^+ ATPases)[1], and forms a homooligomeric, ring-shaped structure (5, 6). Lon contributes to protein quality control surveillance in mitochondria by degrading preferentially oxidatively-modified or misfolded proteins before they aggregate (7–9). In bacteria, in addition to proteolysis of damaged proteins, Lon also plays a key role in turnover of specific unstable proteins involved in a variety of biological processes (3, 4). Similarly, the steroidogenic acute regulatory protein StAR, several subunits of cytochrome *c* oxidase, and oxidized mitochondrial aconitase are known to be Lon substrates in animal mitochondria (10–14).

In addition to its proteolytic function, mitochondrial Lon has the ability to bind DNA in vitro (15–17), and has been shown to interact with mtDNA in human cultured cells (18). However, the physiological role of DNA binding by Lon is not clear. In yeast, loss of PIM1, which is the ortholog of animal Lon protease, causes mtDNA deletion, impairs mitochondrial gene expression and results in respiratory deficiency (19, 20). A role for Lon has been postulated in mtDNA replication, transcription, and/or maintenance, but this remains to be validated. Lon was demonstrated to be a component of mitochondrial nucleoids, which are protein: DNA complexes formed to package mtDNA (21, 22). The major protein component of mtDNA nucleoids is mitochondrial transcription factor A (TFAM or mtTFA) (23, 24). TFAM contains two high mobility group (HMG) amino acid sequence boxes; it binds to mtDNA both specifically and nonspecifically (25). TFAM is essential for mtDNA transcription and for mtDNA packaging in mtDNA maintenance (26–30). Interestingly, mtDNA and TFAM levels are interdependent, such that knockdown of TFAM results in mtDNA depletion, and reduction of mtDNA copy number causes reduction of TFAM levels (26, 29, 31).

In this study, we investigated the role of Lon protease in regulating mtDNA maintenance and transcription, and the protein components of mitochondrial nucleoids in cultured cells. Our results argue strongly that Lon modulates mtDNA biogenesis by the selective degradation of TFAM.

Results

Overexpression of Lon Reduces TFAM Levels and mtDNA Copy Number. Mitochondrial localization of the *Drosophila Lon* gene product (CG8798) was confirmed in Schneider cells by fluorescence microscopy (Fig. S1). Next, *Drosophila Lon* was subcloned into the inducible expression vector pMt/Hy under the control of the metallothionein promoter. The resulting expression vector, pMt/Lon/Hy, was introduced into Schneider cells, and stable cell lines harboring this plasmid were cultured in media with or without 0.2 mM $CuSO_4$. After 10 d of incubation in the presence of copper, immunoblot analysis indicated a fivefold increase in Lon relative to that in the uninduced control cells (Fig. 1*A*). In contrast, expression of β-tubulin, used as a control protein, was unchanged. Levels of protein components of the mitochondrial nucleoid were measured by immunoblotting of cells carrying no plasmid, pMt/Hy, or pMt/Lon/Hy.

Overexpression of Lon reduced the level of TFAM to 75% of that in the control cells (Fig. 1 *A*, *B*). Levels of other proteins localized in mitochondrial nucleoids, including mtTFB2, mtDNA helicase, pol γ-α, and mtSSB, were not changed. We used Southern blots to quantify relative mtDNA copy number in the Lon overexpression cells. We found that the relative mtDNA copy number in the overexpression cells was ~0.7-fold of that in the control cells (Fig. 1*C*). Northern blots were used to quantify the relative expression of the *Cytb, ND4, and 12S rRNA* genes in cells grown for 10 d in the presence or absence of copper. Overexpression of Lon did not show any significant changes on these mitochondrial transcript levels as compared to the control cells (Fig. 1*D*). Furthermore, TFAM mRNA levels were unchanged by Lon overexpression, indicating that the reduction in TFAM protein levels in the knockdown cells does not result from the reduction of TFAM mRNA.

RNAi-Dependent Knockdown of Lon Increases TFAM, Mitochondrial DNA Copy Number, and Mitochondrial Transcription. We reduced the abundance of Lon by expressing a metallothionein-inducible *Lon*-targeted RNAi species from the plasmid pMt/invLon/Hy. The RNA species produced a form of dsRNA hairpin homolo-

Author contributions: Y.M. and L.S.K. designed research; Y.M. performed research; Y.M., Y.G., and L.S.K. analyzed data; and Y.M. and L.S.K. wrote the paper.

The authors declare no conflict of interest.

*This Direct Submission article had a prearranged editor.

[1]To whom correspondence should be addressed. E-mail: lskaguni@msu.edu.

This article contains supporting information online at www.pnas.org/lookup/suppl/doi:10.1073/pnas.1008924107/-/DCSupplemental.

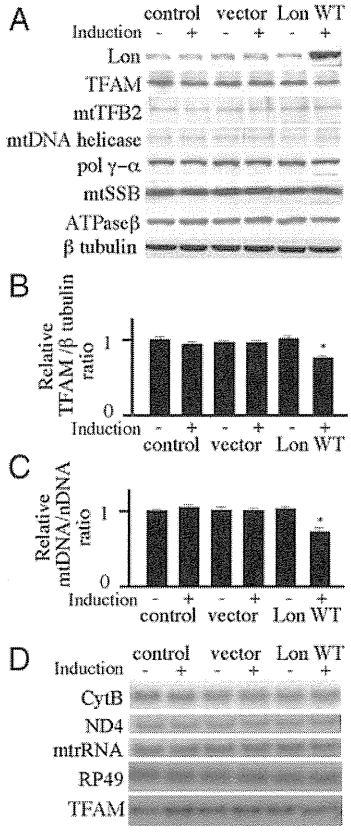

Fig. 1. Expression of *Drosophila* Lon protease in Schneider cells. Schneider cells with no plasmid (control) or carrying pMt/Hy (vector) or pMt/Lon/Hy (Lon WT) were cultured for 10 d in the presence or absence of 0.2 mM CuSO4. (*A*) Protein extracts (20 μg) were fractionated by 7.5%, 10.5%, or 13.5% SDS-PAGE, transferred to nitrocellulose filters and probed with antibodies against Lon protease, TFAM, mtTFB2, mtDNA helicase, pol γ-α, mtSSB, ATPase β, or β tubulin as indicated. (*B*) The TFAM/ β tubulin ratio was quantitated by normalizing TFAM protein levels to β tubulin protein levels as described under *Materials and Methods*. Error bars indicate means ± standard error of three independent experiments. The asterisk indicates $P < 0.05$ in comparison to control. (*C*) Total DNA (10 μg) was extracted from Schneider cells or Schneider cells carrying pMt/Hy or pMt/Lon/Hy that were cultured for 10 d in the presence of 0.2 mM CuSO4. DNA was digested with XhoI, fractionated in a 0.7% agarose/ TBE gel, and then blotted to a nylon membrane. The membrane was hybridized with a radiolabeled probe for CytB, and then stripped and rehybridized with radiolabeled probe for the histone gene cluster as a control. The relative mtDNA copy number was quantitated as described under *Materials and Methods*. Error bars indicate means ± standard error of three independent experiments. The asterisk indicates $P < 0.05$ in comparison to control. (*D*) Total RNA (10 μg) was extracted from Schneider cells or Schneider cells carrying pMt/Hy or pMt/Lon/Hy after 10 d of culture in the presence or absence of 0.2 mM CuSO4. RNA was fractionated in a 1.2% agarose/formaldehyde gel, blotted to nylon membrane, and hybridized with radiolabeled probes for the mitochondrial transcripts *12S rRNA, ND4*, and *Cytb*, the nuclear transcript *RP49*, and *TFAM*.

gous to *Lon*. Schneider cells stably expressing pMt/invLon/Hy showed the accumulation of oxidized proteins in mitochondria (Fig. S2), but the knockdown cells could be maintained for at least 6 mo under normal culture conditions. Schneider cells stably expressing pMt/invLon/Hy were cultured for 10 d in the absence or presence of 0.2 mM $CuSO_4$. Immunoblot analysis of copper-treated cells showed that cells carrying pMt/invLon/Hy expressed >10-fold less Lon than cells carrying the control vector (Fig. 2*A*). Even in the uninduced condition, the cells carrying pMt/invLon/Hy suppressed expression of Lon by >10-fold, most likely due to leaky expression (32–35). In contrast, expression of β-tubulin was unchanged. Again levels of mitochondrial nucleoid proteins were measured by immunoblotting of cells carrying no plasmid, pMt/Hy, or pMt/invLon/Hy. Depletion of Lon increased the protein levels of TFAM and mtTFB2 ~1.4-fold relative to their levels in the control cells (Fig. 2*A*, *B*). At the same time, the levels of other mitochondrial nucleoid proteins were not changed significantly. Next, relative mtDNA copy number was measured in the knockdown cells in the presence or absence of copper and found to be ~1.3-fold higher than in the control cells (Fig. 2*C*). These results suggest that the increase in mtDNA copy number results from the increased TFAM levels.

Northern blots were used to quantitate relative expression of the *Cytb, ND4*, and *12S rRNA* genes in cells grown for 10 d in the presence or absence of copper. Basal expression of Lon-targeted RNAi increased the transcript levels of *Cytb, ND4*, and *12S rRNA* to ~1.4-fold that of the control cells (Fig. 2*D*). This increase in the mitochondrial transcripts may result from either the increase in mtTFB2 or mtDNA copy number, or both. In contrast, the level of transcripts from the nuclear gene *RP49* was unchanged by Lon knockdown. Similar to that observed upon the overexpression of Lon, TFAM mRNA levels were unchanged in the Lon knockdown cells (Fig. 2*D*), indicating that the increase in TFAM pro-

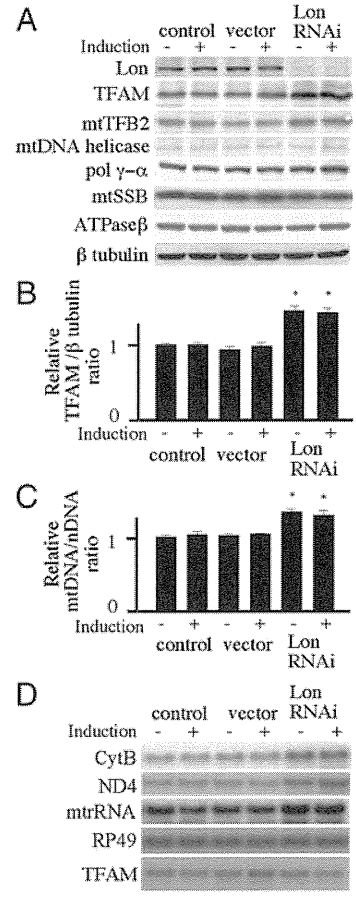

Fig. 2. Expression of *Drosophila* Lon-targeted RNAi in Schneider cells. Schneider cells with no plasmid (control) or carrying pMt/Hy (vector) or pMt/invLon/Hy (Lon RNAi) were cultured for 10 d in the presence or absence of 0.2 mM CuSO4. (*A*) Immunoblot analysis was carried out as described in the legend to Fig. 1*A*. (*B*) The TFAM/β tubulin ratio was quantitated by normalizing TFAM protein levels to β tubulin protein levels as described under *Materials and Methods*. Error bars indicate means ± standard error of three independent experiments. The asterisk indicates $P < 0.05$ in comparison to control. (*C*) Relative mtDNA copy number was determined as described in the figure legend to Fig. 1*C*. Error bars indicate means ± standard error of three independent experiments. The asterisk indicates $P < 0.05$ in comparison to control. (*D*) Northern blot analysis using *12S rRNA, ND4, Cytb, RP49*, and *TFAM* was carried out as described in the legend to Fig. 1*D*.

tein in the knockdown cells does not result from an increase in the steady-state level of TFAM transcripts.

Lon Regulates mtDNA-Dependent TFAM Degradation in Schneider Cells. Our data show that Lon regulates TFAM levels and mtDNA copy number. Because of the interdependent relationship of TFAM and mtDNA, we asked whether or not Lon degrades TFAM directly. To do so, we cultured the cell lines in the presence of ethidium bromide (EtBr), an inhibitor of mtDNA replication. In the control cells, EtBr treatment results in a rapid reduction of mtDNA copy number, and TFAM protein levels were also reduced, albeit more slowly than that of mtDNA (Fig. 3 *A*, *B*). At the same time, TFAM mRNA levels were unchanged (Fig. S3). Because the levels of other mitochondrial nucleoid proteins were not affected by mtDNA depletion with EtBr, we conclude that TFAM is depleted selectively following mtDNA reduction. In the Lon overexpression cells, EtBr treatment also resulted in the reduction of mtDNA (Fig. 3*B*). Interestingly, here the reduction of TFAM was faster than in the control cells (Fig. 3*A*). EtBr treatment also caused mtDNA depletion in the Lon knockdown cells. However in this case, the relative level of TFAM protein was increased 1.2-fold (Fig. 3*A*), while again TFAM mRNA levels were unchanged (Fig. S3). Similar to the control cells, the levels of other mitochondrial nucleoid proteins were unchanged in the EtBr treated Lon knockdown cells.

To demonstrate conclusively the proteolytic role of Lon in mtDNA-dependent TFAM degradation, we established a cell line expressing a Lon mutant carrying a S880A amino acid substitution, in which the conserved serine in the proteolytic active site was replaced by alanine. The cell line expressing Lon S880A showed severe retardation of TFAM degradation following mtDNA depletion, likely because overexpression of Lon S880A results in a dominant negative phenotype that is caused by the formation of mixed oligomeric forms (Fig. S4). Taken together, our data show clearly that Lon is responsible for specific degradation of TFAM.

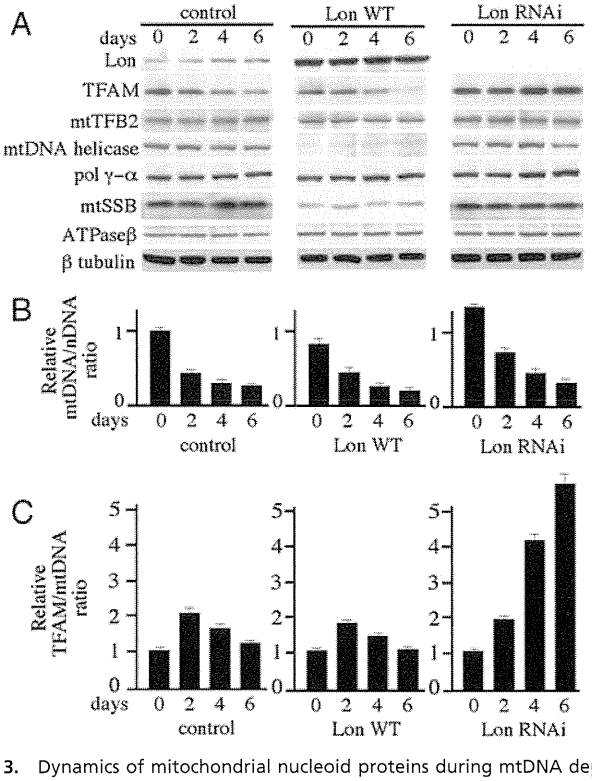

Fig. 3. Dynamics of mitochondrial nucleoid proteins during mtDNA depletion in Lon overexpressing or knockdown Schneider cells. Schneider cells with no plasmid (control) or carrying pMt/Lon/Hy (Lon WT) or pMt/invLon/Hy (Lon RNAi) were cultured for 6 d in the presence of 200 ng/mL EtBr. The cells were harvested prior to EtBr treatment (0 d) and after 2, 4, and 6 days of EtBr treatment. (*A*) Immunoblot analysis was carried out as described in the legend to Fig. 1*A*. (*B*) Relative mtDNA copy number was determined as described in the legend to Fig. 1*C*. Error bars indicate means ± standard error of two independent experiments. (*C*) The TFAM/ mtDNA ratio was quantitated by normalizing TFAM levels to relative mtDNA copy number. Error bars indicate means ± standard error of two independent experiments.

What Is the Physiological Role of Lon Degradation of TFAM? We sought to investigate the functional significance of the specific degradation of TFAM in mtDNA-depleted cells. In control cells treated with EtBr, the TFAM:mtDNA ratio was raised transiently, and then reverted to normal levels within 6 d (Fig. 3*C*). However, Lon knockdown cells did not recover a normal TFAM:mtDNA ratio. In mammalian cells, overexpression of TFAM causes suppression of mitochondrial transcription (36). We confirmed this phenomenon in Schneider cells overexpressing TFAM under the control of the metallothionein promoter (Fig. S5), and find that suppression occurs in cells containing a TFAM:mtDNA ratio >2 (Fig. 4). Interestingly, the highest overexpression level showed depletion of mtDNA copy number in addition to transcriptional suppression. We thus hypothesized that Lon regulates mtDNA transcription by stabilizing the cellular TFAM:mtDNA ratio. To document this hypothesis, we measured mitochondrial transcript levels in mtDNA-depleted cells. Because EtBr also inhibits mtDNA transcription, we instead induced mtDNA depletion by knockdown of mtDNA replication factors and in particular, the catalytic subunit of mitochondrial DNA polymerase and the mtDNA helicase. Control and Lon knockdown cells were cultured for 10 d with dsRNA targeted against these proteins or GFP as a control, and the relevant protein levels were then evaluated by immunoblotting (Fig. 5*A*). The cells cultured with GFP dsRNA showed no change in these protein levels, whereas in the cell lines cultured with the mtDNA helicase or mtDNA polymerase dsRNAs, mtDNA copy number was reduced to ~60% of that in the control cells (Fig. 5*B*). After the dsRNA treatments, the TFAM levels decreased to 75% in control cells, but increased 1.2-fold in the Lon knockdown cells (Fig. 5*A*). After the dsRNA treatments, the TFAM:mtDNA ratio in the control cells was increased ~1.3-fold relative to the control cells alone, and the ratio in the Lon RNAi cells was increased ~2.5-fold (Fig. 5*C*). Mitochondrial transcripts in the control cells were unchanged with or without dsRNA treatment (Fig. 5*D*). However, the transcript levels in mtDNA-depleted Lon RNAi cells were reduced to 47%–60% of those in the mtDNA-depleted cells that showed transcript levels equivalent to 66%–84% of the

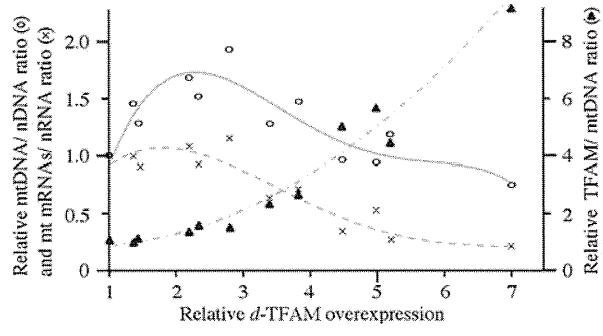

Fig. 4. Expression of TFAM in Schneider cells. Relative ratio of mtDNA copy number (*open circles, solid line*), mt mRNAs/nRNA (*crosses, dotted line*), and TFAM/mtDNA (*filled triangles, dashed line*) were measured at different overexpression levels of TFAM in Schneider cells as indicated. Relative mtDNA copy number was determined as described in the legend to Fig. 1*C*. The mt mRNAs/nRNA ratio was quantitated by normalizing mitochondrial transcript abundance (*ND4* and *Cyt b*) to that of nuclear *Rp49*. TFAM/mtDNA ratio was quantitated by normalizing TFAM protein levels to relative mtDNA copy number.

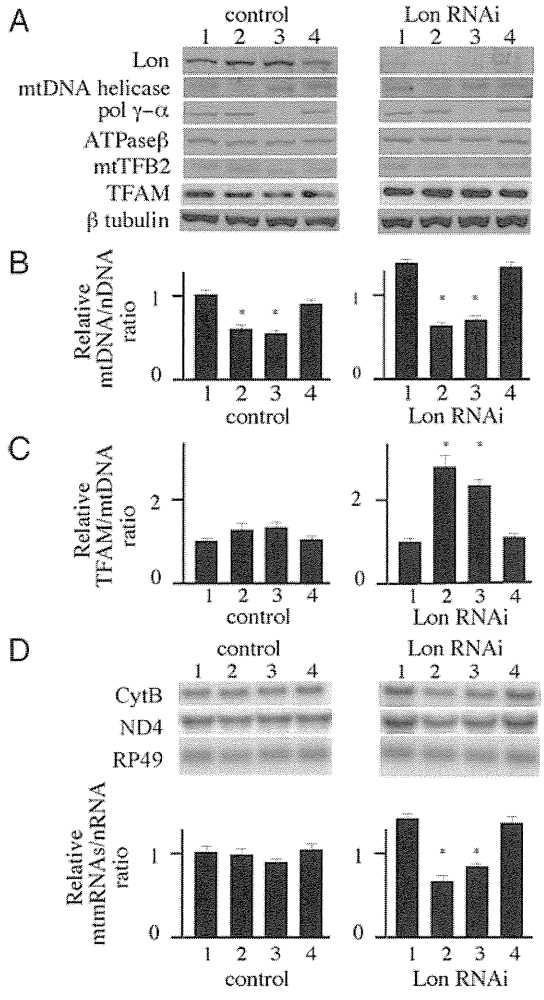

Fig. 5. Effects of Lon knockdown on mitochondrial transcript levels after mtDNA depletion in Schneider cells. Schneider cells carrying no plasmid (control) and or pMt/invLon/Hy (Lon RNAi) were cultured for 10 d in the presence or absence of dsRNA of mtDNA helicase, pol γ-α, or GFP as control. (*A*) Immunoblot analysis was carried out as described in the legend to Fig. 1*A*. (*B*) Relative mtDNA copy number was determined as described in the legend to Fig. 1*C*. Error bars indicate means ± standard error of two independent experiments. The asterisk indicates $P < 0.05$ in comparison to the control. (*C*) The ratio of TFAM/mtDNA was determined as described in the legend to Fig. 3*C*. Error bars indicate means ± standard error of two independent experiments. The asterisk indicates $P < 0.05$ in comparison to each cell that was cultured in the absence of dsRNA. (*D*) Northern blot analysis using *ND4, Cytb, and RP49* was carried out as described in the legend to Fig. 1*D*. Relative mitochondrial mRNA levels were quantitated by normalizing *ND4* and *Cytb* abundance to that of RP49. Error bars indicate means ± SE of two in dependent experiments. The asterisk indicates $P < 0.05$ in comparison to the control.

control cells. Interestingly, the reduced mitochondrial transcript levels were lower than that of control cells. Together, these results indicate that Lon regulates mitochondrial transcription by controlling the TFAM:mtDNA ratio.

Discussion

We have established that Lon knockdown cell lines express <10% of endogenous Lon protein levels, yet these cells grow for at least 6 mo. In human fibroblast cells, depletion of Lon over 4 d resulted in apoptotic cell death (37, 38), whereas Lon knockdown in human colon carcinoma cells allows survival for at least 15 d (18). Thus, the effects of Lon depletion may be species- or cell type- specific. As in a recent report with human rhabdomyosarcoma cells (39), depletion of Lon protease in *Drosophila* Schneider cells results in an increase in the levels of oxidized proteins in mitochondria, indicating that Lon is responsible for degradation of oxidized mitochondrial proteins, and suggesting that variations in cell viability as a result of Lon depletion may reflect varying cellular tolerances for oxidative damage to mitochondrial proteins.

It is known that TFAM protein levels are reduced coincident with mtDNA depletion in animal cells, but the mechanism for this phenomenon is unclear (31). Here, we show that Lon is responsible for degradation of TFAM upon mtDNA depletion. Moreover, Lon may be also responsible for TFAM degradation under normal conditions, because the cellular level of TFAM varies in concert with Lon levels. These findings imply that TFAM turnover is strongly dependent on Lon protease function. In addition to TFAM, we found that the mtTFB2 level is increased in Lon knockdown cells, so it may also be a specific substrate for the Lon protease. Other mitochondrial biogenesis proteins tested were unchanged appreciably in either Lon knockdown or overexpression cells. In *Escherichia coli*, some substrates for Lon overlap those of other AAA^+ proteases such as the ClpP protease; notably, the ClpP ortholog in animal cells comprises another major protease in the mitochondrial matrix space (2, 3, 40). Therefore, the depletion of mitochondrial Lon may be compensated partially by mitochondrial ClpP protease. Alternatively, the residual Lon in knockdown cells may be sufficient to degrade its protein targets.

We found that mitochondrial transcripts in Lon knockdown cells are increased moderately in association with an increase of TFAM and mtTFB2 levels. Previous studies showed that the relative levels of mtDNA and TFAM are not critical to observe stimulation of mitochondrial transcription in *Drosophila* Kc167, and Schneider cells (29, 35). We suggest that in contrast, increase of mtTFB2, which is essential for mitochondrial transcription, may be responsible for up-regulation of mitochondrial transcription.

We show that degradation of TFAM by Lon protease is facilitated by mtDNA depletion. Interestingly, a similar phenomenon was reported in *Bacillus subtilis*. *B. subtilis* LonA, which is the ortholog of Lon, is involved in degradation of the structural maintenance of chromosomes protein (SMC), and the degradation of SMC is facilitated by DNAase treatment (41). Although the mechanisms by which Lon recognizes its target proteins are not well understood, a recent report showed that *E. coli* Lon recognizes specific aromatic residue-rich sequences that are hidden in the hydrophobic cores of native structures, but are accessible in unfolded structures (42). Interestingly, the HMG boxes in TFAM contain four conserved aromatic residues within a hydrophobic core, and these residues may be masked when TFAM binds DNA (25, 27, 29). Another possible explanation is that TFAM not bound to mtDNA becomes exposed to oxidative stress, whereas TFAM bound to mtDNA comprises part of the core of the mitochondrial nucleoids, and is thus surrounded by other proteins (43). Mitochondrial Lon has the ability to bind DNA and localizes in mitochondrial nucleoids (15–18). Our current hypothesis is that excess, free TFAM is degraded by Lon before the TFAM binds DNA. Alternatively, it seems possible, albeit more complicated, that excessive DNA compaction resulting from binding of high TFAM levels signals the degradation of TFAM by DNA-bound Lon. Further experiments are warranted to address these and other possibilities, and to clarify the link between the DNA-binding activity of Lon and TFAM turnover.

Suzuki and colleagues showed that mtDNA copy number was unchanged after 15 d of Lon knockdown in human colon carcinoma cells (18). This model differs from ours, in which we observe an increase in mtDNA copy number. We established our Lon knockdown cells over a period of 8 wks and because of leaky expression from the inducible promoter in the RNAi vector, Lon depletion was already ongoing prior to the 10 d induction

period. Thus, one possible explanation for the difference we observe is that TFAM accumulation may be slower in their model and consequently, increased mtDNA copy number might not have been apparent. Another possible explanation is that compensation by other proteases such as ClpP (2, 40) might effect TFAM degradation in the Lon-depleted human colon carcinoma cells.

We found that upon EtBr treatment, the TFAM:mtDNA ratio is nearly restored within 6 d in both control and Lon overexpressing cells, whereas restoration did not occur in Lon knockdown cells. Moreover, TFAM turnover resulting from mtDNA depletion by EtBr treatment is strongly reduced in cells overexpressing a protease-deficient Lon variant, which shows a dominant negative effect. Similar results involving restoration of normal TFAM/ mtDNA ratios were produced in the case of knockdowns of mtDNA helicase and mtDNA polymerase, though there the reduction of mtDNA is lower as compared to that upon EtBr treatment. Until stabilization occurs, excess overexpression of TFAM results in reduction of mitochondrial transcript levels; notably, in TFAM overexpressing cells, ratios of TFAM:mtDNA >2 show inhibitory effects on mitochondrial transcription. In the case of knockdown of mtDNA helicase or mtDNA polymerase, mitochondrial transcription levels are unchanged in control cells upon mtDNA depletion, whereas Lon knockdown cells showed a similar reduction in mitochondrial transcripts. Upon knockdown of mtDNA helicase or mtDNA polymerase, the TFAM:mtDNA is ~1.3 in control cells and >2 in Lon knockdown cells, consistent with the observations in TFAM overexpression cells. Because there are environmental conditions under which mtDNA copy number is known to vary, such as during development and upon drug treatment (44, 45), transient Lon degradation of excess TFAM would be important to maintain normal mitochondrial transcription levels. We conclude that the TFAM:mtDNA ratio is crucial for both mtDNA biogenesis and homeostasis, and that Lon stabilizes the TFAM:mtDNA ratio by degradation of excess TFAM. With the example of TFAM, we provide direct evidence of the physiological role of Lon protease activity in mtDNA maintenance in animal cells, warranting future study of its potential involvement in the surveillance and turnover of other proteins involved in mtDNA replication, transcription, and translation.

Materials and Methods

Preparation of Lon Antibody. A recombinant protein corresponding to amino acids Asp613 to Ser838 of *Drosophila* Lon (CG8798) was used to immunize rabbits to obtain polyclonal antibody.

Preparation of Inducible Plasmids Expressing Lon, TFAM, and Lon-Targeted RNAi. The plasmid pMt/Lon/Hy, in which Lon is regulated by the metallothionein promoter and the plasmid pMt/invLon/Hy, which carries an inverted repeat of a nucleotide sequence from *Lon* cDNA that is transcribed from the metallothionein promoter were constructed as described in the *SI Text*. Plasmid pMt/TFAM/Hy is as described previously (35).

Generation and Induction of Stable Cell Lines. *Drosophila* Schneider S2 cells were cultured at 25 °C in *Drosophila* Schneider Medium (Invitrogen) supplemented with 10% FBS. Cells were subcultured to 3×10^6 cells/mL every fifth day. Cells were transfected using Effecten (QIAGEN). Hygromycin-resistant cells were selected with 200 μg/mL hygromycin. Cells were passaged for 8 wks in hygromycin-containing medium and then cultured in standard medium. The cell lines were grown to a density of 3×10^6/mL and then treated with 0.2 mM $CuSO_4$ to induce expression from the metallothionein promoter.

Immunoblotting. Total cellular protein (20 μg per lane) was fractionated by 13.5%, 10.5%, or 7.5% SDS-PAGE and transferred to nitrocellulose filters. Immunoblotting was performed as described previously (46). Protein bands were visualized using ECL Western blotting reagents (Amersham). ECL luminescence was quantified on a Kodak Image Station 4000R. Antibodies against *Drosophila* mtSSB (47), TFAM (29), Pol γ-α (48), mtDNA helicase (32), ATPase β (32), mtTFB2 (35), and β tubulin (E7) (Developmental Studies Hybridoma Bank) were prepared and used as described. The ratio of the signals for TFAM and β tubulin was used to estimate the relative protein levels of TFAM. The TFAM immunoblotting experiments shown in Figs. 1, 2, 3, and 5 were performed two or thee times with each of the two or three independent cell lines carrying each plasmid construct, including control (no plasmid). The data presented represent one such experiment, and the quantitation is provided for the duplicate or triplicate experiments from one of two or thee cell lines.

Northern and Southern Blotting. Northern blotting was performed as described previously (46), and the data were analyzed using a PhosphoImager (Molecular Dynamics). The signal for *RP49* was used to normalize mitochondrial transcripts.

Southern blotting was performed as described previously (32), and the data were analyzed using a PhosphoImager (Molecular Dynamics). Blots were probed with radiolabeled DNAs for the mitochondrial gene *Cytb* and the nuclear histone gene cluster. The ratio of the signals for these two genes was used to estimate the relative copy number of mtDNA. The Northern and Southern blot experiments shown in Figs. 1, 2, 3, 4, and 5 were performed two or thee times with each of the two or three independent cell lines carrying each plasmid construct, including control (no plasmid). The data presented represent one such experiment, and the quantitation is provided for the duplicate or triplicate experiments from one of two or thee cell lines.

RNA Interference. To generate double-stranded RNA (dsRNA) for RNAi, sequences directed against the protein to be silenced were amplified by PCR from each cDNA. Each primer used in the PCR contained a T7 RNA promoter followed by sequences specific for the targeted genes. The following primer sets were used for each protein: mtDNA helicase for GTAATACGACTCACTATAGGGCATGGAAAATGAGACGCGC and GTAATACGACTCACTATAGGGGATTGCTGACTAGAACCGC; DNA polymerase γ-α for TAATACGACTCACTATAGGGTGCCTACGCCTGCGGTGAGC and TAATACGACTCACTATAGGGCTCCAATGCTCGACTAAGAC; GFP for GTAATACGACTCACTATAGGGGGAGAAGAACTTTTCACTGG and GTAATACGACTCACTATAGGGTCTGCTAGTTGAACGCTTC. PCR products were used as templates for in vitro transcription using the T7 Megascript RNAi kit (Ambion). 3×10^7 S2 *Drosophila* tissue culture cells were plated into a T25 flask in 5 mL of medium without FBS. 100 μg of dsRNA was added and mixed by swirling. After 30 min, 5 mL of media containing 20% FBS was added. The cells were collected after 5 d culture and repeat dsRNA treatment. After 5 d after second dsRNA treatment, the cells were harvested for the analysis.

ACKNOWLEDGMENTS. We thank Marcos Oliveira for critical comments on the manuscript. This work was supported by National Institutes of Health (NIH) Grant GM45295 (to L.S.K.), and by a research grant (21A-6) for Nervous and Mental Disorders, a Health and Labour Science Research Grant on Intractable Diseases, and a grant of the Comprehensive Research Project on Health Sciences Focusing on Drug Innovation from the Ministry of Health, Labour, and Welfare of Japan (to Y.G.).

1. Lee I, Suzuki CK (2008) Functional mechanics of the ATP-dependent Lon protease-lessons from endogenous protein and synthetic peptide substrates. *Biochim Biophys Acta* 1784:727–735.
2. Koppen M, Langer T (2007) Protein degradation within mitochondria: versatile activities of AAA proteases and other peptidases. *Crit Rev Biochem Mol Biol* 42:221–242.
3. Tsilibaris V, Maenhaut-Michel G, Van Melderen L (2006) Biological roles of the Lon ATP-dependent protease. *Res Microbiol* 157:701–713.
4. Chandu D, Nandi D (2004) Comparative genomics and functional roles of the ATP-dependent proteases Lon and Clp during cytosolic protein degradation. *Res Microbiol* 155:710–719.
5. Park SC, et al. (2006) Oligomeric structure of the ATP-dependent protease La (Lon) of *Escherichia coli*. *Mol Cells* 21:129–134.
6. Stahlberg H, et al. (1999) Mitochondrial Lon of *Saccharomyces cerevisiae* is a ring-shaped protease with seven flexible subunits. *Proc Natl Acad Sci USA* 96:6787–6790.
7. Voos W (2009) Mitochondrial protein homeostasis: the cooperative roles of chaperones and proteases. *Res Microbiol* 160:718–725.
8. Van Melderen L, Aertsen A (2009) Regulation and quality control by Lon-dependent proteolysis. *Res Microbiol* 160:645–651.
9. Friguet B, Bulteau AL, Petropoulos I (2008) Mitochondrial protein quality control: implications in ageing. *Biotechnology Journal* 3:757–764.
10. Granot Z, et al. (2007) Turnover of mitochondrial steroidogenic acute regulatory (StAR) protein by Lon protease: the unexpected effect of proteasome inhibitors. *Mol Endocrinol* 21:2164–2177.
11. Fukuda R, et al. (2007) HIF-1 regulates cytochrome oxidase subunits to optimize efficiency of respiration in hypoxic cells. *Cell* 129:111–122.
12. Ondrovicova G, et al. (2005) Cleavage site selection within a folded substrate by the ATP-dependent Lon protease. *J Biol Chem* 280:25103–25110.

13. Hori O, et al. (2002) Transmission of cell stress from endoplasmic reticulum to mitochondria: enhanced expression of Lon protease. *J Cell Biol* 157:1151–1160.
14. Bota DA, Davies KJ (2002) Lon protease preferentially degrades oxidized mitochondrial aconitase by an ATP-stimulated mechanism. *Nat Cell Biol* 4:674–680.
15. Lu B, et al. (2003) The ATP-dependent Lon protease of Mus musculus is a DNA-binding protein that is functionally conserved between yeast and mammals. *Gene* 306:45–55.
16. Fu GK, Markovitz DM (1998) The human LON protease binds to mitochondrial promoters in a single-stranded, site-specific, strand-specific manner. *Biochemistry* 37:1905–1909.
17. Liu T, et al. (2004) DNA and RNA binding by the mitochondrial Lon protease is regulated by nucleotide and protein substrate. *J Biol Chem* 279:13902–13910.
18. Lu B, et al. (2007) Roles for the human ATP-dependent Lon protease in mitochondrial DNA maintenance. *J Biol Chem* 282:17363–17374.
19. Van Dyck L, Pearce DA, Sherman F (1994) PIM1 encodes a mitochondrial ATP-dependent protease that is required for mitochondrial function in the yeast *Saccharomyces cerevisiae*. *J Biol Chem* 269:238–242.
20. Suzuki CK, Suda K, Wang N, Schatz G (1994) Requirement for the yeast gene LON in intramitochondrial proteolysis and maintenance of respiration. *Science* 264:273–276.
21. Kucej M, Butow RA (2007) Evolutionary tinkering with mitochondrial nucleoids. *Trends Cell Biol* 17:586–592.
22. Cheng X, et al. (2005) PDIP38 associates with proteins constituting the mitochondrial DNA nucleoid. *J Biochem* 138:673–678.
23. Garrido N, et al. (2003) Composition and dynamics of human mitochondrial nucleoids. *Mol Biol Cell* 14:1583–1596.
24. Alam TI, et al. (2003) Human mitochondrial DNA is packaged with TFAM. *Nucleic Acids Res* 31:1640–1645.
25. Gangelhoff TA, Mungalachetty PS, Nix JC, Churchill ME (2009) Structural analysis and DNA binding of the HMG domains of the human mitochondrial transcription factor A. *Nucleic Acids Res* 37:3153–3164.
26. Kanki T, et al. (2004) Architectural role of mitochondrial transcription factor A in maintenance of human mitochondrial DNA. *Mol Cell Biol* 24:9823–9834.
27. Matsushima Y, et al. (2003) Functional domains of chicken mitochondrial transcription factor A for the maintenance of mitochondrial DNA copy number in lymphoma cell line DT40. *J Biol Chem* 278:31149–31158.
28. Falkenberg M, et al. (2002) Mitochondrial transcription factors B1 and B2 activate transcription of human mtDNA. *Nat Genet* 31:289–294.
29. Goto A, Matsushima Y, Kadowaki T, Kitagawa Y (2001) *Drosophila* mitochondrial transcription factor A (d-TFAM) is dispensable for the transcription of mitochondrial DNA in Kc167 cells. *Biochem J* 354:243–248.
30. Larsson NG, et al. (1998) Mitochondrial transcription factor A is necessary for mtDNA maintenance and embryogenesis in mice. *Nat Genet* 18:231–236.
31. Seidel-Rogol BL, Shadel GS (2002) Modulation of mitochondrial transcription in response to mtDNA depletion and repletion in HeLa cells. *Nucleic Acids Res* 30:1929–1934.
32. Matsushima Y, Kaguni LS (2007) Differential phenotypes of active site and human autosomal dominant progressive external ophthalmoplegia mutations in *Drosophila* mitochondrial DNA helicase expressed in Schneider cells. *J Biol Chem* 282:9436–9444.
33. Matsushima Y, Adan C, Garesse R, Kaguni LS (2007) Functional analysis by inducible RNA interference in *Drosophila* melanogaster. *Methods in Molecular Biology* 372:207–217.
34. Matsushima Y, Adan C, Garesse R, Kaguni LS (2005) *Drosophila* mitochondrial transcription factor B1 modulates mitochondrial translation but not transcription or DNA copy number in Schneider cells. *J Biol Chem* 280:16815–16820.
35. Matsushima Y, Garesse R, Kaguni LS (2004) *Drosophila* mitochondrial transcription factor B2 regulates mitochondrial DNA copy number and transcription in schneider cells. *J Biol Chem* 279:26900–26905.
36. Pohjoismaki JL, et al. (2006) Alterations to the expression level of mitochondrial transcription factor A, TFAM, modify the mode of mitochondrial DNA replication in cultured human cells. *Nucleic Acids Res* 34:5815–5828.
37. Ngo JK, Davies KJ (2007) Importance of the Lon protease in mitochondrial maintenance and the significance of declining Lon in aging. *Ann N Y Acad Sci* 1119:78–87.
38. Bota DA, Ngo JK, Davies KJ (2005) Downregulation of the human Lon protease impairs mitochondrial structure and function and causes cell death. *Free Radical Biol Med* 38:665–677.
39. Ngo JK, Davies KJ (2009) Mitochondrial Lon protease is a human stress protein. *Free Radical Biol Med* 46:1042–1048.
40. Yu AY, Houry WA (2007) ClpP: a distinctive family of cylindrical energy-dependent serine proteases. *FEBS Lett* 581:3749–3757.
41. Mascarenhas J, et al. (2005) Dynamic assembly, localization, and proteolysis of the *Bacillus subtilis* SMC complex. *BMC Cell Biol* 6:28.
42. Gur E, Sauer RT (2009) Degrons in protein substrates program the speed and operating efficiency of the AAA+ Lon proteolytic machine. *Proc Natl Acad Sci USA* 106:18503–18508.
43. Bogenhagen DF, Rousseau D, Burke S (2008) The layered structure of human mitochondrial DNA nucleoids. *J Biol Chem* 283:3665–3675.
44. Foster C, Lyall H (2008) HIV and mitochondrial toxicity in children. *J Antimicrob Chemother* 61:8–12.
45. Moraes CT (2001) What regulates mitochondrial DNA copy number in animal cells? *Trends Genet* 17:199–205.
46. Matsushima Y, Farr CL, Fan L, Kaguni LS (2008) Physiological and biochemical defects in carboxyl-terminal mutants of mitochondrial DNA helicase. *J Biol Chem* 283:23964–23971.
47. Farr CL, Wang Y, Kaguni LS (1999) Functional interactions of mitochondrial DNA polymerase and single-stranded DNA-binding protein. Template-primer DNA binding and initiation and elongation of DNA strand synthesis. *J Biol Chem* 274:14779–14785.
48. Wang Y, Farr CL, Kaguni LS (1997) Accessory subunit of mitochondrial DNA polymerase from *Drosophila* embryos. Cloning, molecular analysis, and association in the native enzyme. *J Biol Chem* 272:13640–13646.

Supporting Information

Matsushima et al. 10.1073/pnas.1008924107

SI Text

SI Materials and Methods. ***Preparation of inducible plasmids expressing cMyc-Lon and the Lon S880A mutant.*** The plasmid pMt/Lon/Hy, in which Lon is regulated by the metallothionein promoter, was constructed as follows: a fragment of *Drosophila* Lon cDNA was amplified by PCR using as 5′-primer 5′- GGGCTCGAGTGCGAGTGGATATTGCTTTC -3′ and as 3′-primer 5′- GCGCACTAGTATTACAAGTCTTCTTCAGAAATAAGCTTTTGAGAATAAGGCCACGTCTC -3′. The PCR fragment was cleaved by XhoI and SpeI and subcloned.

pMt/S880A/Hy was constructed from pMt/Lon/Hy by site directed mutagenesis using the following pair of primers: 5′-AGATGGCCCCGCTGCGGGCATC -3′ and 5′- GATGCCCGCAGCGGGGCCATCT -3′.

Detection of carbonylated proteins. The OxyBlot procedure (Millipore) was used to perform immunoblot detection of oxidatively modified proteins by the generation of carbonyl groups. Ten micrograms of protein were used for each reaction. Carbonyl groups in mitochondrial protein samples (10 μg) were derivatized to 2,4-dinitrophenylhydrazone (DNP-hydrazone) by reaction with 2,4-dinitrophenylhydrazine. Carbonylated proteins were detected by immunoblot analysis using an anti-DNP antibody.

Indirect immunofluorescence. Indirect immunofluorescence was performed as described (1) with anti-c-Myc monoclonal antibody (Sigma) and Alexa Fluor 488 anti-mouse IgG (Molecular Probes).

Preparation of inducible plasmids expressing Lon, TFAM, and Lon-Targeted RNAi. The plasmid pMt/Lon/Hy, in which Lon is regulated by the metallothionein promoter, was constructed as follows: a fragment of *Drosophila* Lon cDNA was amplified by PCR using as 5′-primer 5′- GGGCTCGAGTGCGAGTGGATATTGCTTTC -3′ and as 3′-primer 5′- GCGCACTAGTCTAAGAATAAGGCCACGTCTC -3′. The PCR fragment was cleaved by XhoI and SpeI and subcloned. The plasmid pMt/TFAM/Hy was as described previously (2). The plasmid pMt/invLon/Hy carries an inverted repeat of a nucleotide sequence from *Lon* cDNA that is transcribed from the metallothionein promoter. The insert in pMt/invLon/Hy was generated from two PCR-amplified fragments of *Lon* cDNA. One fragment has terminal XhoI and EcoRI sites and was prepared using the following pair of primers: 5′- GCGCCTCGAGACTAGTGGGATGATTCCAACGGGGAT -3′ (forward) and 5′- GCGCGAATTCGGGATCGATTCCGCTTGATCAGTGCTTTG -3′(reverse). A second fragment has terminal SpeI and EcoRI sites and was prepared using the primers 5′- GCGCCTCGAGACTAGTGGGATGATTCCAACGGGGAT -3′ (forward) and 5′- GCGCGAATTCAAAAAGCTTTCCGCTTGATCAGTGCTTTG -3′ (reverse). The two PCR products were ligated and cloned into the pMt/Hy vector cleaved with XhoI and SpeI.

1. Goto A, Matsushima Y, Kadowaki T, Kitagawa Y (2001) *Drosophila* mitochondrial transcription factor A (d-TFAM) is dispensable for the transcription of mitochondrial DNA in Kc167 cells *Biochem J* 354:243–248.

2. Matsushima Y, Garesse R, Kaguni LS (2004) *Drosophila* mitochondrial transcription factor B2 regulates mitochondrial DNA copy number and transcription in schneider cells. *J Biol Chem* 279:26900–26905

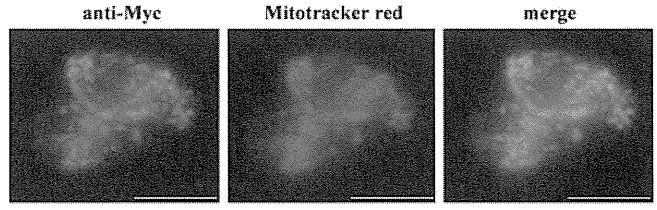

Fig. S1. Overexpression of *Drosophila* Lon in Schneider cells. Immunocytochemistry was performed on Schneider cells that were transiently transfected with pMK/Lon-Myc/Hy using anti-c-Myc monoclonal antibody (Sigma), and counterstained with Mitotracker Red.

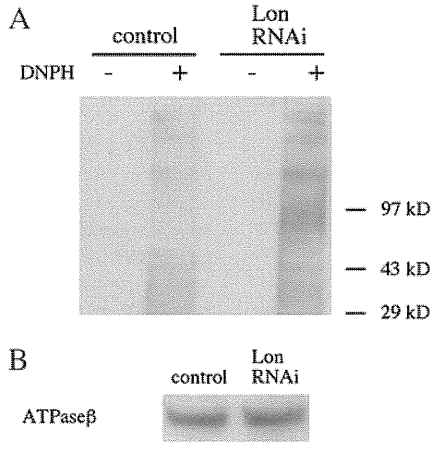

Fig. S2. Protein oxidation status in mitochondria from Lon knockdown cells. Mitochondrial fractions were prepared from Schneider cells carrying no vector (control) or pMt/invLon/Hy (Lon RNAi). (*A*) Detection of oxidized protein was performed using the Oxyblot protocol (Millipore). Mitochondrial protein extracts (10 μg) were incubated in the presence or absence of 2,4-dinitrophenylhydrazine (DNPH) to derivatize protein carbonyl groups. After fractionation by 4%–10% gradient SDS-PAGE, the proteins were transferred to a nitrocellulose filter, and oxidized proteins were detected with antibody against DNP. (*B*) Mitochondrial protein extracts (10 μg) were fractionated by 12% SDS-PAGE, transferred a nitrocellulose filter and probed with affinity-purified rabbit antiserum against ATPase β as a control.

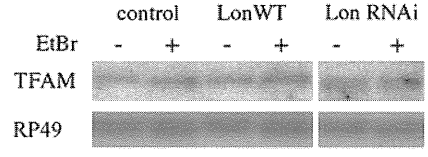

Fig. S3. Unchanged TFAM mRNA levels in Schneider cells upon EtBr treatment. After 6 d culture, Total RNA was isolated from Schneider cells with no plasmid (control) or carrying pMt/Lon/Hy (Lon) or pMt/invLon/Hy (Lon RNAi) that were cultured for 6 d in the presence or absence of 200 ng/mL EtBr. Northern blot analysis using *TFAM* and *RP49* probes was carried out as described in the legend to Fig. 1*D*.

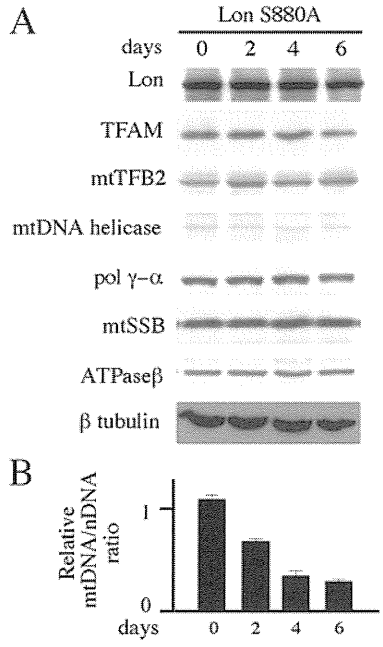

Fig. S4. Steady-state levels of mitochondrial nucleoid proteins during mtDNA depletion in Lon S880A- overexpressing Schneider cells. Schneider cells carrying pMt/S880A/Hy (S880A) were cultured for 6 d in the presence of 200 ng/mL EtBr. The cells were harvested prior to and after EtBr treatment at 0, 2, 4, and 6 days. (*A*) Immunoblot analysis was carried out as described in the legend to Fig. 1*A*. (*B*) Relative mtDNA copy number was determined as described in the legend to Fig. 1*C*.

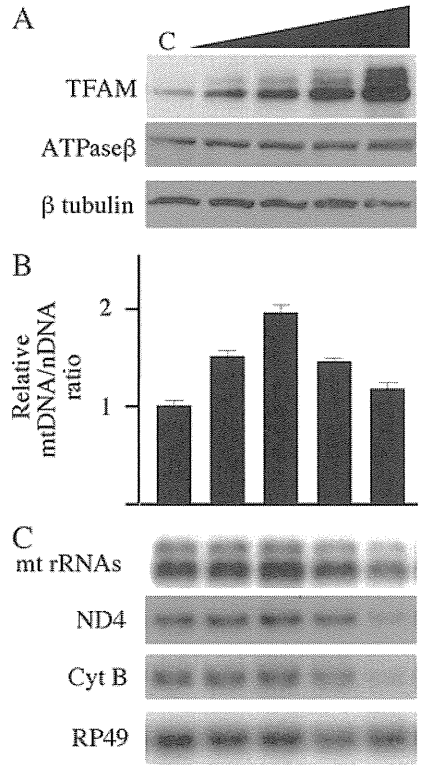

Fig. S5. Expression of *Drosophila* TFAM in Schneider cells. Schneider cells (*C*) or cells carring pMt/TFAM/Hy were grown for 10 d in the presence of 0, 0.05, 0.1, or 0.4 mM CuSO4. (*A*) Immunoblot analysis was carried out as described in the legend to Fig. 1*A*. (*B*) Relative mtDNA copy number was determined as described in the legend to Fig. 1*C*. Error bars indicate means ± standard error of two independent experiments. (*C*) Northern blot analysis using *12S rRNA, ND4, Cytb*, and *RP49* was carried out as described in the legend to Fig. 1*D*.

Reversible Infantile Respiratory Chain Deficiency: A Clinical and Molecular Study

Masakazu Mimaki, MD, PhD,[1] Hideyuki Hatakeyama, PhD,[1] Hirofumi Komaki, MD,[1,2] Mina Yokoyama, MD,[2] Hidee Arai, MD,[3] Yohei Kirino, PhD,[4] Tsutomu Suzuki, PhD,[4] Ichizo Nishino, MD, PhD,[5] Ikuya Nonaka, MD, PhD,[2,5] and Yu-ichi Goto, MD, PhD[1,2]

Objective: To characterize the clinical features and clarify the pathogenicity of "benign cytochrome *c* oxidase deficiency myopathy."
Methods: The study included 8 patients with the phenotype of this disease. Six patients underwent muscle biopsies and all the 8 underwent mitochondrial DNA analyses. To confirm the pathogenicity of the detected mitochondrial DNA mutation, we performed northern blot analysis, using muscle specimens, and blue native polyacrylamide gel electrophoresis and respiratory chain enzyme activity assay of transmitochondrial cell lines (cybrids).
Results: Clinical symptoms were limited to skeletal muscle and improved spontaneously in all cases; however, 2 siblings had basal ganglia lesions. In all patients, we identified a homoplasmic m.14674T>C or m.14674T>G mitochondrial transfer RNA-glutamate mutation. Northern blot analysis revealed decreased levels of mitochondrial transfer RNA-glutamate molecules. Muscle specimens and cybrids derived from patients showed decreased activity of respiratory complexes IV, and/or I, III; however, this was normal in naive myoblasts.
Interpretation: Identification of a novel m.14674T>G mutation in addition to m.14674T>C indicated the importance of this site for disease causation. Analyses of cybrids revealed the pathogenicity of m.14674T>C mutation, which resulted in defects of cytochrome c oxidase and multiple respiratory chain enzymes. Furthermore, patients with basal ganglia lesions provided new insights into this disease, in which only skeletal muscle was thought to be affected. Normal respiratory chain enzyme activities in naive myoblasts suggested the compensatory influence of nuclear factors, which may be a clue to understanding the mechanisms of spontaneous recovery and low penetrance in families carrying the mutation.

ANN NEUROL 2010;68:845–854

Mitochondrial cytochrome *c* oxidase (COX) a multisubunit assembly present in the inner membrane. is responsible for the terminal event in electron transport.[1] Deficiency of this enzyme is one of the most frequent and clinically heterogeneous causes of respiratory chain deficiency.[1–3] An increasing number of genetic defects have been identified in both mitochondrial DNA (mtDNA) and nuclear DNA.[4–12] The onset of COX deficiency is variable, and most patients show progressive clinical symptoms.

Benign infantile COX deficiency, known as "benign COX deficiency myopathy," is very rare and distinct because of its unusual disease course, which is characterized by clinical and pathological improvement. These patients have lactic acidosis, hypotonia, hyporeflexia, and generalized muscle weakness from early infancy—features similar to those seen in the classical fatal infantile form.[13,14] The symptoms, however, improve spontaneously after 1 year of age.[15–20] The molecular defect in this disease was previously unknown; however, Horvath et al.[21] have recently reported a single homoplasmic m.14674T>C mutation.

In this study, we investigated 8 patients with benign infantile COX deficiency to evaluate its clinical and pathological characteristics and disease outcome. We detected

View this article online at wileyonlinelibrary.com. DOI: 10.1002/ana.22111

Received Jan 21, 2010, and in revised form Apr 25, 2010. Accepted for publication May 28, 2010.

Address correspondence to Dr. Goto, National Institute of Neuroscience, National Center of Neurology and Psychiatry (NCNP), 4-1-1 Ogawahigashi, Kodaira, Tokyo 187-8502, Japan.. E-mail: goto@ncnp.go.jp

From the [1]Department of Mental Retardation and Birth Defect Research, National Institute of Neuroscience, National Center of Neurology and Psychiatry (NCNP), Tokyo, Japan; [2]Department of Child Neurology, National Center Hospital of Neurology and Psychiatry, National Center of Neurology and Psychiatry (NCNP), Tokyo, Japan; [3]Department of Neurology, Chiba Children's Hospital, Chiba, Japan; [4]Department of Chemistry and Biotechnology, Graduate School of Engineering, University of Tokyo, Tokyo, Japan; and [5]Department of Neuromuscular Research, National Institute of Neuroscience, National Center of Neurology and Psychiatry (NCNP), Tokyo, Japan.

Additional Supporting Information can be found in the online version of this article.

the reported homoplasmic mutation in 6 patients and identified a novel T to G base change at the same nucleotide point (np) in 2 patients. Furthermore, we performed biochemical analyses on the transmitochondrial cell lines (cybrids) to confirm the pathogenicity of the mutation and influence of nuclear factors.

Patients and Methods

Case Reports

Subjects of this study were 8 (3 male and 5 female) benign infantile COX deficiency patients (Table 1). Patient 7 and 8 were siblings. Patient 4 has been described previously in a Japanese report.[20] Six patients underwent muscle biopsies and the muscle specimens for patients 7 and 8 were not available. We obtained written informed consent to perform muscle biopsies, biochemical studies, and/or molecular analyses from parents of all patients.

None of the patients' parents were consanguineous. All patients were born uneventfully after a normal pregnancy. All patients presented as "floppy infants" with muscle weakness and hypotonia from early infancy, but symptoms improved with age, particularly after 1 year of age. The follow-up period ranged from 18 months to 15 years. We documented developmental milestones, history of tube feeding and respirator management, complications (short stature, hearing loss, renal dysfunction, liver dysfunction, cardiac failure, diabetes mellitus, seizure, and mental status), laboratory data (lactate levels in blood and cerebrospinal fluid [CSF], and creatinine kinase [CK] in blood), and neuroimaging.

Histopathological Studies

Muscle biopsy from biceps brachii was performed at mean age of 5.6 months (range, 3–9 months). Serial frozen sections were stained with hematoxylin and eosin, modified Gomori trichrome, succinate dehydrogenase (SDH), COX, and ATPase stains.

mtDNA Analysis

For mtDNA analysis, total DNA was extracted from muscle specimens of 6 patients (patients 1–6) and lymphocytes of patients 7 and 8. Southern blot and long polymerase chain reaction (PCR) analyses were performed to detect mtDNA rearrangements, as described previously.[22,23] Total mtDNA sequencing was performed as described previously.[24] The sequence data were compared with the Human Mitochondrial DNA Revised Cambridge Reference Sequence (MITOMAP; http://www.mitomap.org). To confirm m.14674T>C and m.14674T>G mutations by restriction fragment length polymorphism (RFLP) analysis, PCR fragments were digested by *BclI* and *NlaIII*, respectively (see the section on RFLP analysis in Supporting Information Methods).

Mitochondrial Transfer RNA Analysis

For transfer RNA (tRNA) analysis, total RNA was extracted by Isogen (Nippon Gene, Toyama, Japan) from muscle specimens, naive myoblasts, and cybrids obtained by fusing enucleated myoblasts of patient 6 carrying m.14674T>C mutation with human osteosarcoma 143B/TK-cells lacking mtDNA as described previously.[25]

To evaluate the molecular size and quantity of tRNA-glutamate ($tRNA^{Glu}$), we performed northern blot analysis using total RNA extracted from muscle specimens of patients 3 and 4, and normal infants. Patients 3 and 4 had the m.14674T>G mutation and m.14674T>C mutation, respectively. Samples of total RNA were electrophoresed and northern hybridization was performed using a DNA probe specific for mitochondrial $tRNA^{Glu}$. $tRNA^{Glu}$ amounts were normalized by the amount of mitochondrial tRNA-Leu (UUR) and nuclear-encoded 5S ribosomal RNA (rRNA)[26] (see the section on Quantification of $tRNA^{Glu}$ in Supporting Information Methods).

To evaluate aminoacylation levels of tRNA, we performed acid polyacrylamide gel electrophoresis (PAGE). Total RNA samples were extracted from cybrids and 143B/TK-cells (normal control), prepared to be aminoacyl-tRNAs or forcibly deacylated tRNAs according to the literature,[27] and electrophoresed to separate aminoacyl-$tRNA^{Glu}$ and uncharged $tRNA^{Glu}$ (see the section on acid PAGE in Supporting Information Methods).

Enzymatic Activity of Respiratory Chain Complexes of Naive Myoblasts, Cybrids, and Muscle Specimens

Enzymatic activity of individual mitochondrial respiratory complexes was determined using isolated mitochondria obtained from cultured primary myoblasts and cybrids derived from patient 6, according to Trounce et al.[28] with modifications. Skeletal muscle specimens from patients 3, 4, and 6 were also available. The activities of complexes I, II, III, and IV and citrate synthase (CS) were measured using spectrophotometric assays. All samples were measured at least in duplicate and averaged.

Blue Native PAGE and Western Blot for Immunodetection

Mitochondrial proteins were isolated from cultured 143B/TK cells and cybrids derived from patient 6.[29] The mitochondrial proteins (100μg) were solubilized in sample buffer containing 0.5% (w/v)*n*-dodecyl-β-D-maltoside. Electrophoresis was performed on 3% to 12% polyacrylamide gels (Invitrogen, Carlsbad, CA).[29,30] Following blue native PAGE (BN-PAGE), gels were blotted on polyvinylidene fluoride membranes using the iBlot transfer system (Invitrogen). Subunit-specific mouse monoclonal antibodies (Molecular Probes, Eugene, OR) were used to immunodetect protein complexes. The cocktail of primary antibodies included 39kDa (complex I) (0.5 μg/mL), 70kDa (complex II) (0.5μg/ml), core II (complex III) (0.5 μg/ml), subunit I (complex IV) (2.5 μg/ml), and subunit β(complex V) (0.5 μg/ml). After removing the cocktail of primary antibodies, alkaline phosphatase-conjugated anti-mouse secondary antibody was reacted and nitroblue tetrazolium chloride–derived chromogenic detection was performed.